POLITECNICO DI TORINO

Master of Science in Aerospace Engineering

Master Thesis

Mission Design and Modeling of Space Manipulators for In-Orbit Servicing Missions.

Supervisors:

Dr. Elisa Capello

Ing. Andrea Bacchetta

Candidate:

Pietro Chevallard

Marzo 2019

Abstract

In near future, in-orbit operations will change the vision of space as a "static" place, where each spacecraft's lifetime is programmed from launch to retirement. Thanks to its capabilities, when need arises, operators could amend the initial planned mission of a satellite, by repairing or upgrading its payload, or simply extending its life expenctancy by refuelling, or, at least, have it deorbited. This topic is also part of a bigger initiative, aimed to foster suistainability in space, to grant future manned and unmanned mission a safe and clean environment to operate in. In this context, this thesis is focused on pointing out a possible in-orbit servicing mission, on a ESA owned satellite, in order to accomplish goals such as deorbiting or refuelling. The targets, selected through a trade-off, resulted to be the best in terms of ΔV budgets and mission time. Secondly, is developed, at an early stage, the model of a spaceraft-mounted robotic arm, capable of operating on spacecrafts. The manipulator is modeled using Simulink and following Lagrangian formulation, aiming to highlight and evaluate the reactions on the base induced by the manipulator's motion. The results showed that this effects does not impact partcularly on the base dynamics and that they could be easily balanced by an ordinary control system.

The thesis was developed during an internship at TAS-I (Thales Alenia Space Italia) in Turin in cooperation with the GNC (Guidance, Navigation and Control) group.

Contents

List of Figures

List of Tables

Chapter 1

Introduction

1.1 General Overview

The unregulated exploitation of the space surrounding the Earth is causing long term effects that will negatively affect the whole space industry. Clean Space, an initiative of the European Space Agency (ESA), started in 2012, has the goal to reduce the impact of space industry on both space and Earth environment; one of its objectives is the reduction of the amount of space debris. Reaching this objective will also require in-orbit servicing capabilities. In-orbit servicing is a wide-ranging topic that spans from refuelling or maintenance to deorbiting satellites that have reached their end-of-life.

The increasing production of space debris has acquired more and more importance in the past few years, due to the threat that they represent for manned and unmanned missions.Suitable actions seems necessary in order to avoid the risk that space debris completely occupy fundamental orbits and their density becomes too high for accomplishing safe launches. Unoperative or uncontrolled satellites aren't the only source of danger for space missions; also debris in the microscale, due to their velocity and thus their energy, are a major threat; for example during the STS-7 mission of the Space Shuttle in 1983, a paint flake only $0.2\,mm$ in diameter hit the Challenger making a crater $4\,mm$ wide in its window [18]. After the first accidents, researchers developed two types of countermeasures: collision avoidance systems and Whipple shields. Collision avoidance is used when debris are too big to be shielded and is performed changing the orientation or the position of the spacecraft. Whipple shields, on the contrary, are made up of a bumper spaced some centimeters from the internal wall and are effective only against small debris whose speed ranges between 3 and $18\frac{km}{s}$. The purpose of this particular shielding is to break up and disperse the incoming object, in order to spread its energy over a larger wall area which has more chances to withstand it.

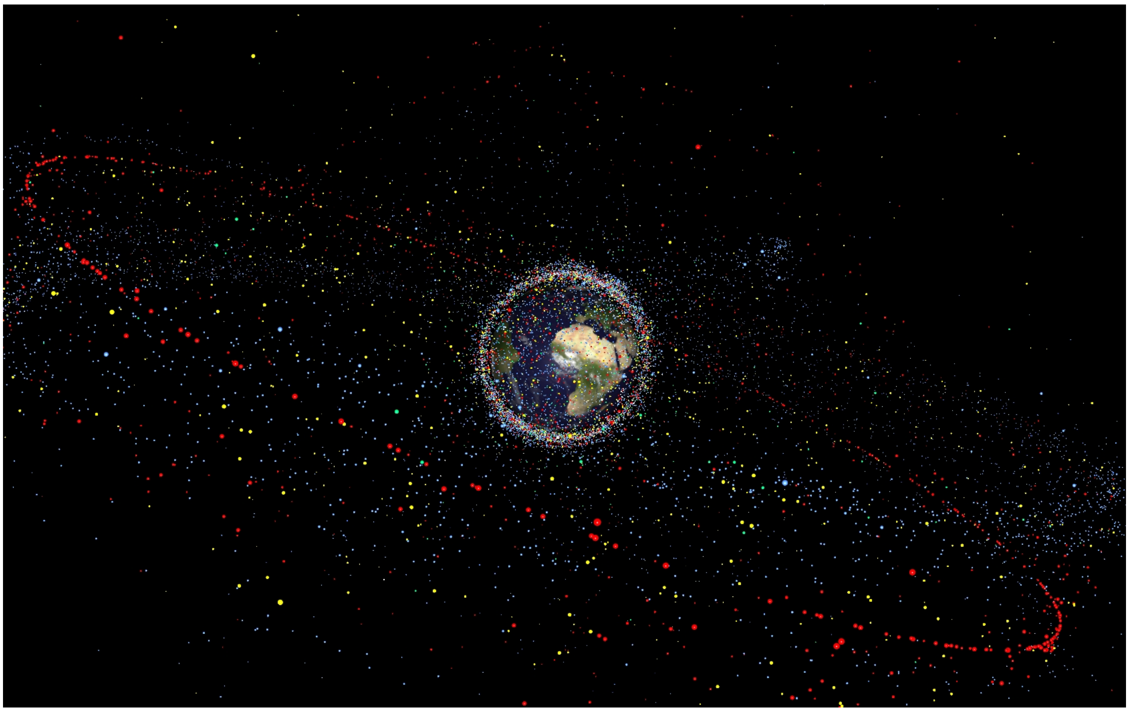

Figure 1.1: Distribution of debris around the Earth

The hazardous condition caused by debris was firstly analyzed by NASA scientist Donald J. Kessler in 1978 [18]. His studies show that with enough debris density, a collision between two of them could cause a cascade where each impact increases the likelihood of further collisions. This possibility of a collisional cascading effect is called Kessler Syndrome, and is acquiring more importance since the quantity of space debris has increased during the years. Potential triggering events occurred in the last 20 years, like the Chinese Fengyun anti-satellite test or the Iridium-Cosmos collision [18], in which the number of debris dramatically rose. This issue highlights the necessity of a precise regulation concerning space debris for future missions in order to avoid fatal accidents and to grant secure access to orbits surrounding the Earth.

1.2 Clean Space

Several attempts to reduce the environmental impact of human activities in space have been made during the past years. ESA's Clean Space initiative is the European answer to this issue, which aims to create a more sustainable space industry through three different solutions: EcoDesign, CleanSat and e.Deorbit. EcoDesign means designing missions considering their environmental impact and fostering green technologies; CleanSat addresses the reduction of the production of debris, requiring end-of-life satellite disposal to be planned in future missions; e.Deorbit solution was developed to reduce the quantity of space garbage currently orbiting around the Earth. The initial objective of e.Deorbit was to capture an ESA owned satellite and burn it up in a controlled reentry. Not all these solutions have maintained the same objective since the launch of Clean Space; e.Deorbit debris removal mission has recently been revised as a servicing vehicle, with the capacity of performing a variety of different tasks. In orbit servicing operations include refuelling, refurbishing and reboosting of satellites already in orbit as well as end-of-life satellite disposal through a controlled reentry or the relocation into a graveyard orbit.

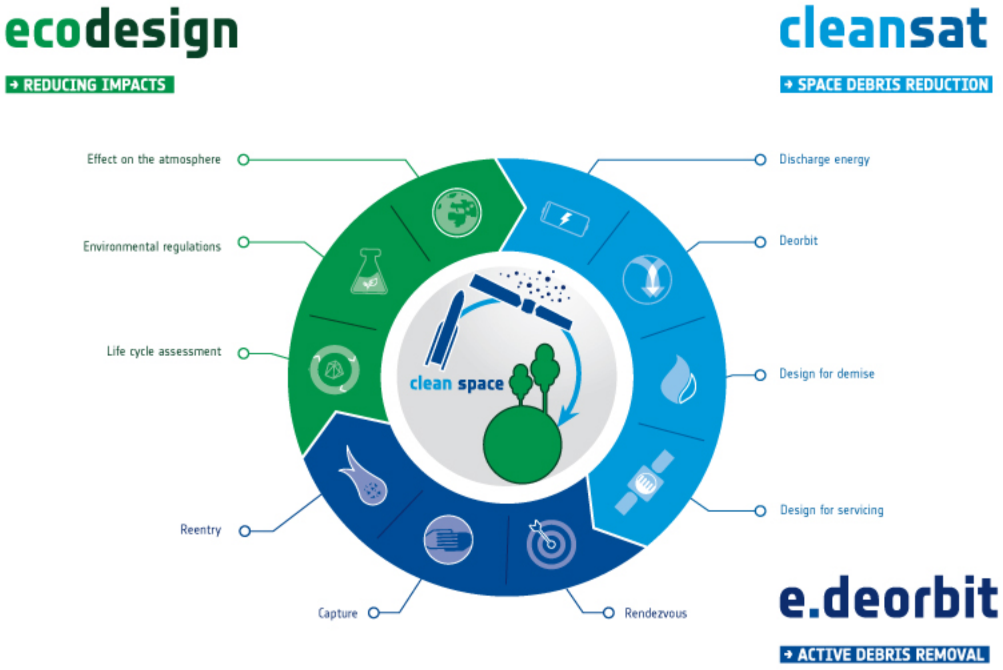

Figure 1.2: Clean space infographic - Courtesy of ESA

Thales Alenia Space Italia has chosen to take part to this initiative and through an internal research is developing a solution that could accomplish e.Deorbit goals. To achieve its purposes the vehicle must be equipped with one or more devices capable of capturing a satellite and operating on it. The capture phase could be successfully performed using different techniques, depending on the service that has to be carried out. Regarding the removal of a debris from its orbit, a net, an harpoon or a robotic arm are three different suitable ways; if the goal is instead to service a satellite to extend its life, a robotic arm seems to be the best way to accomplish the task. The use of a robotic arm, mounted on a spacecraft, has proven to be the best option for the capture and servicing thanks to its flexibility in carrying out different tasks. To extend the operational life and to provide the disposal of a satellite, the servicer can also be also equipped with a life-extension/deorbiting kit [20], which will be attached on the target. This kit consists of a solid rocket engine, to produce thrust, coupled with a small attitude control system that allows the satellite to be operational for several months after the application of the kit; moreover the kit provides control of the spacecraft even if it is no longer operational.

Anyway, even if the use of a servicer to deorbit satellites will help to reduce the number of debris, it is not a sustainable approach to the issue but only a temporary solution; in the future, end-of-life satellite disposal has to be planned before the launch, to prevent further generation of debris and related hazards.

Starting from the considerations above, this study will focus on finding a suitable ESA owned satellite to service, in order to answer a RFI(Request For Information) from ESA to TAS. It will also concern on creating a model of a space manipulator capable of performing fine operations, in order to study its interactions with the base, to understand the challenges arosen by this particular spacecraft.

1.3 Chapter Overview

The thesis is composed of 7 chapters including the conclusions; each of these deals with differents issues and topics, following, from the first to the last, the work logic of the subjects treated.

The following chapter describes various kinds of In-Orbit Servicing and, one one side, characterizes the chaser and the targets for the servicing, on the other, outlines the equations used and the assumptions made for the comparison which will follow.

The third chapter deals with a preliminary comparison of the selected missions, which after a trade-off based on ΔV budgets and mission duration, outlines the chosen cases; in the end, are shown the mass, ΔV and mission's duration budgets. Alongwith the chapter ends the first part of the thesis, which regarded the answer to a RFI(Request For Information) sent by ESA to TAS.

Fourth chapter introduce space manipulators and their history, with a brief overview of Lagrangian and Newton-Euler formulations followed by a block description of the model. In the fifth chapter are detailed both formulations, outlining the geometric and dynamical properties of the system and in the end are specified the direct and inverse kynematics control modes. The sixth chapter analizyes the simulations' results, for the deployment and tracking phases, showing how the manipulator interacts with its base. Last chapter concludes the work, showing which improvements could be made in future for refining the model.

Chapter 2

In Orbit Servicing

2.1 General Overview

In the second half of 2018, the European Space Agency (ESA) has asked Industry to propose an Outline Concept for cleaner space and to demonstrate the capacities for in orbit satellite removal.Main objective of this initiative are:

- to perform the removal of ESA satellite(s) as a precursor of in-orbit servicing;
- to demomstarte technologies, functions and operational know-how to perform other in orbit services;
- to achieve the above by means of service contract(s) to provide opportunity to space industry to enter into this new space market.

For this purpose, several possible missions were considered, in order to identify a feasible demonstration mission.
Capturing satellites presents different challenges, whether the Target is cooperative or not, due to issues in avoiding collision between Target and Chaser; even if grasping of controlled Targets it's easier, in-orbit servicing operations such as maintenance or refueling have far more complexity than simple disposal of inoperative satellites. Therefore, it was chosen to perform only deorbiting, of which two types are possible:

1. a targeted re-entry in Earth Atmosphere, and
2. disposal into a graveyard orbit.

Both of them could be performed into two different ways:

1. directly by the Chaser, or
2. through the deorbiting/life extension kit [20].

All these possibilities present similar challenges and they have been considered in this study and in performing trade-offs among the various cases.
When possible, reentry in Earth atmosphere is performed: atmospheric drag and high temperatures will destroy the disposed satellite, cleaning the orbits around the Earth. The drag becomes relevant at about 80 km above the sea level, therefore the starting orbit of the Target must be a LEO (Low Earth Orbit) orbit or with perigee near LEO altitudes. If this condition is not satisfied, the ΔV becomes too high and a graveyard orbit results a more practical solution. The spacecraft/Chaser intended to accomplish the mission will be brought in orbit by Ariane 6 launcher and will be supplied with particular equipment specifically designed for its mission; three robotic arms and a life extension/deorbiting kit (as in chapter 1) will be mounted on it. The kit presents also some uncertainties about its resistance to space environment for long periods of time, due to the degradation effects caused by radiation on the solid propellant that could affect its performances. Depending on the task that they have to accomplish, two types of arm can be identified: a catcher arm to capture the Target spacecraft and operate on it safely and two coupled arms to secure the Target (in fact, as soon as the Chaser captures the Target, flexibility of the resulting total assembly becomes a relevant issue and it is necessary to provide adequate stiffness). Foldable solar arrays were chosen to supply the Chaser because retracting them in critical phases, such as capture, would reduce collision risk with the Target. To provide thrust, a hybrid propulsion system was designed; it is composed of a chemical thruster for the impulsive maneuvers (RendezVous and Capture - RVC, inclination changes, etc.) and an electrical thruster, for the transfer between distant orbits.

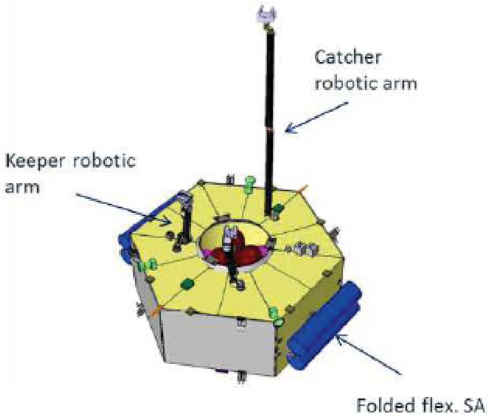

Figure 2.1: Chaser spacecraft - Courtesy of TAS

2.2 Mission Characterization

Initially, the objective was to service only ESA-owned satellites; later the mission was extended also to private sector for possible customers in order to foster sustainability. The Targets were chosen basing on their mass and their orbit, in order to remove potential sources of large numbers of debris. As shown in Table 4.1 most of them weigh at least $1000kg$, and some of them occupy particular orbits, like SSO (Sun Synchronous Orbit), which are useful for Earth and poles observation. Basing on a TAS internal survey, five different scenarios were evaluated:

- Deorbit Hipparcos and ISO(Infrared Space Observatory) then transfer to GEO(Geostationary Earth Orbit)
- Reorbit Galileo and deorbit ERS-1(European Remote-Sensing Satellite-1)
- Reorbit Galileo and deorbit ERS-1 with Aerobraking
- Deorbit Hipparcos and ERS-1
- Deorbit Hipparcos and ERS-1 with Aerobraking

Most of these Targets are non-operational satellites, i.e. Hipparcos was dismissed in 1993, ISO in 1998, and ERS-1 in 2000, so the mission would focus on deorbiting, performed with or without the help of the kit. Galileo on the contrary is still operational, but due to some issues during the launch phase, it never reached its designated orbit. In this case the mission, more similar to servicing, would accomplish an adjustment and a reorbiting to the planned orbit.

Satellite Name	**Orbit Class**	**Orbit** $[Km]$	**Dry mass** $[Kg]$
HIPPARCOS	GTO	488 x 35790 @ 7,2°	1130
GALILEO 5	MEO	17200 x 23270 @ 49,8°	732,8
ERS-1	LEO	742 x 791 @ 98,5°	2140
ERS-2	LEO	499 x 502 @ 94,6°	2140
ISO	HEO	574 x 70040 @ 5,2°	2475
CHASER	GTO	250 x 35786 @ 6°	TBD

Table 2.1: ESA owned satellites characteristics

Refueling initially was not included, but to achieve further results in terms of "second generation services" and reduce somehow the overall cost of the mission, it was proposed to perform a refuel of the Chaser from the upper stage of the launcher. To reduce the total mass of the Chaser, initially, during this work, was supposed to perform the refueling between the capture of the first and second Targets, but the propellant tanks installed on the upper stage were designed to withstand space

environment only few hours, therefore became necessary to carry it out soon after the release in the designed orbit. Refueling technology has sufficient Technology Readiness Level (TRL) only for Hydrazine while for other types propellant, such as Bi-Prop (Liquid Oxygen and Hydrazine) TRL is too low. This condition forced to choose Hydrazine as propellant for the chemical thruster, while for the electrical was selected Xenon. All the propellants properties thrust and I_{sp} are shown in the Table 2.2 below.
At the very first stage of the project, Aerobraking was not included and was introduced as a technique to lower the orbit, while cruising from one Target to another, without fuel consumption. It is performed lowering the orbit up to $100 - 150\ km$ and using the drag generated by Earth atmosphere to slow down the spacecraft. To avoid damaging, solar arrays must be oriented in the opposite direction with respect to the motion, so that the solar cells aren't exposed to high temperatures. It was assumed to have no fuel consumption during maneuvering, even if is required some attitude control to avoid exposing sensitive parts.

Propellant	I_{sp} $[s]$	**Thrust** $[N]$
Hydrazine	225	$4\,x\,20$
Bi-prop	321	400
Xenon	1980	$224\,x\,10^{-3}$

Table 2.2: Propellants Characteristics

Several equations coming from orbital mechanics were used to compare the considered cases and to obtain the results shown in the following chapter. Even if the analyzed missions are different, in general, the energy required to reach an orbit can be measured in terms of speed variation, as function of the gravitational force. In particular, the velocity differs in module only if the orbit changes shape, while for the other cases it differs only in direction. For all the in-plane impulses, such as rise of the periapsis, the ΔV required comes from the conservation of mechanical energy [16]

$$\frac{V^2}{2} - \frac{\mu}{r} = -\frac{\mu}{2a} \tag{2.1}$$

In which $\mu = 398600\frac{km^3}{s^2}$ is the planetary gravitational constant, r is the distance between the satellite and the focus of the orbit (the center of the Earth), while a is the semi-major axis of the orbit (if the orbit is circular $a = r$).

From 2.1 the ΔV necessary for a change of the perigee could be obtained:

$$\begin{aligned} V_1 &= \sqrt{-\frac{\mu}{a_1} + \frac{2\mu}{r}} \\ V_2 &= \sqrt{-\frac{\mu}{a_2} + \frac{2\mu}{r}} \\ \Delta V &= V_2 - V_1 \end{aligned} \tag{2.2}$$

where V_1 is the current velocity of the spacecraft and V_2 is the desired velocity. In this situation the fuel is burned at the apogee and depending on the direction of the impulse, it is possible to raise or lower the perigee.
When a transfer between two orbits is needed, a Hohmann transfer orbit is used (an elliptical orbit used to transfer between two other orbits that minimizes fuel consumption). Rearranging equation 2.1 allows finding the ΔV necessary to pass from the current orbit to Hohmann and then from Hohmann to desired orbit. Is possible, then, to find directly the three equations that give the overall ΔV

$$\begin{aligned} \Delta V_1 &= \sqrt{\frac{\mu}{r_1}} \left(\sqrt{\frac{2r_2}{2a_H}} - 1 \right) \\ \Delta V_2 &= \sqrt{\frac{\mu}{r_2}} \left(1 - \sqrt{\frac{2r_1}{2a_H}} \right) \\ \|\Delta V_H &= \|\Delta V_1\| + \|\Delta V_2\|\| \end{aligned} \tag{2.3}$$

where r_1 and r_2 refer respectively to the current and desired orbit. Equations 2.3 are applicable only for circular orbits in which $2a_H = r_1 + r_2$; a particular case occurs when two elliptical orbits share a common apse line, in which the transfer is performed through two impulses: one to change perigee's altitude and the other to change apogee's or vice versa, depending on the orbit. To minimize fuel consumption, these maneuvers, as it was said before, are performed at apogee or perigee, whether is necessary to reduce or increase speed, because in these points of the orbit the spacecraft has respectively the lowest and highest speed.
For inclinations changes, on the other hand, the velocity changes only in orientation but not in module, so 2.1 is not applicable and ΔV comes from the cosine law:

$$\begin{aligned} \Delta V &= \sqrt{V_1^2 + V_2^2 - 2V_1 V_2 \cos(\Delta i)} \\ \cos(\Delta i) &= 1 - \sin\left(\frac{\Delta i}{2}\right) \\ \Delta V &= 2V_1 \sin\left(\frac{\Delta i}{2}\right) \end{aligned} \tag{2.4}$$

In which V_1 is supposed to be equal to V_2 and Δi is the change of inclination to perform.

A particular case occurs when an inclination change is combined with a variation of the apse line, in which the ΔV of the coupled maneuver is lower than the sum of the two uncoupled maneuvers and is obtained applying the cosine law as in (2.4), supposing that V_1 is the initial velocity and V_2 the final one.
Once obtained the necessary ΔV for each maneuver, it was possible to evaluate, through Tsiolkovsky rocket equation, the fuel burned to reach the requested velocites. It states that the intial/final mass ratio is related to the ΔV scaled by a factor c:

$$\frac{m_i}{m_f} = e^{-\frac{\Delta V}{c_{exhaust}}} \tag{2.5}$$

in which $c_{exhaust}$ is the exhaust speed of the burned fuel gases. This is a fixed property of the propellant, that therefore must be chosen carefully, according to the characteristics of mission to accomplish.

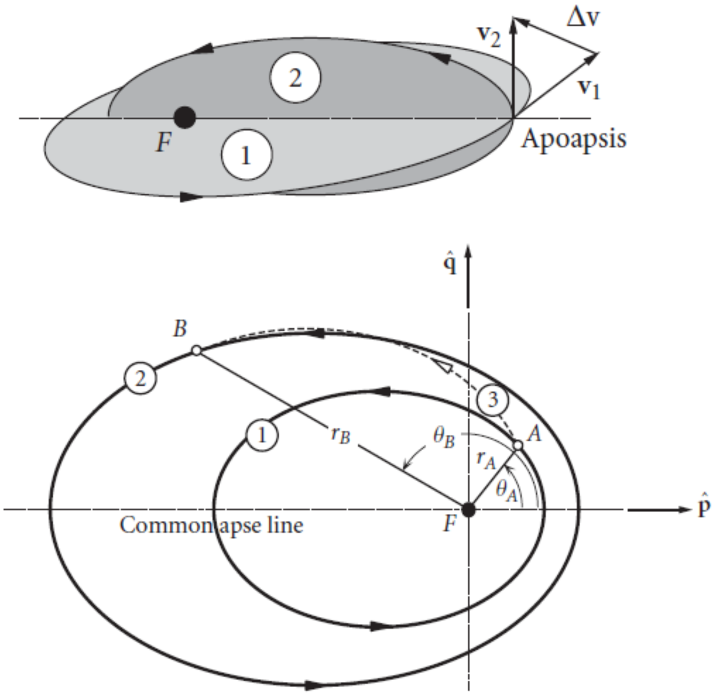

Figure 2.2: Inclination Change and transfer between two elliptical orbit with common apse line

The problem is completely described once the Specific Impulse I_{sp} is defined. It is the thrust compared to sea-level weight rate of fuel consumption and is measured in seconds.

$$I_{sp} = \frac{\dot{m}c_{exhaust}}{\dot{m}g} = \frac{c_{exhaust}}{g} \tag{2.6}$$

It is representative of the efficiency of the propellant: the higher the I_{sp} the higher the ΔV that can be reached. While $c_{exhaust}$ is a fuel unique property, the same I_{sp} can be common to different types of propellants.

Depending on the mission, there are various methods to minimize the fuel consumption, either by choosing lowest ΔVmaneuvers, as in our case, or by using an higher I_{sp} fuel. The last parameter that was taken into account to evaluate the feasibility and the precision of a maneuver was the thrust time or duration of the impulse. The lower it is, more similar to the ideal orbit the real orbit will be, because ideally the impulse is instantaneous

$$t = \frac{\Delta V}{T} \tag{2.7}$$

in which T is the thrust. In case of electric propulsion, it is useful to evaluate the time that the spacecraft will take to travel from an orbit to another; this is necessary to find a first esteem of the mass consumed during the burn:

$$m_{prop} = \frac{T}{gI_{sp}}t \tag{2.8}$$

In electrical engines, in fact, the thrust is applied continuously and therefore Tsiolkovsky's equation loses accuracy, because it does not take into account external forces, such as the gravitational force. Exact solutions to find the mass are too complex for the precision required for this first analysis.

Anyway, to evaluate the cost for each mission, several assumptions were made, mostly to reduce the computation complexity and due to the relatively low level of accuracy required; all the impulsive maneuvers to change orbit are carried out at perigee or apogee and the orbital node is supposed to be coincident with the apse line when an inclination change occurs; moreover, if there is a transfer between two elliptic orbits, they are supposed to have their own apse lines coincident; each rendez-vous costs about $50\frac{m}{s}$.

Some assumptions for the spacecraft were made too, but they vary quite enough depending on the mission's objectives and will be discussed in the following chapter.

Chapter 3

Missions Comparison

3.1 Preliminary Results

Based on the assumptions made in the previous chapter, a comparison between the various missions is performed. The aim is to select the best cases for answer to the RFI; refueling and electric propulsion are not supposed, as Bi-prop is considered as the only choice for chemical thruster due to its performances.
In these cases the chaser is supposed to have a dry mass equal to 600 Kg and the goal is to find the initial mass that allows to carry out the whole mission. An iterative procedure is adopted to find the mass, at first an initial mass is supposed, once found the total m_{prop} it is verified that:

$$m_{prop} + m_{dry} \leqslant m_i \tag{3.1}$$

If equation (3.1) is true the process stopped. The procedure is repeated for each case until convergence. After this assumption it is proceeded to analyze each scenario to find the most suitable to answer the RFI. The first considered scenario is Hipparcos- ISO-GEO which exploits the similar orbits of the 2 satellites to reach them with little cost in terms of ΔV. Once left by launcher in GTO, the chaser will perform an inclination change from 6° to 7,2° at the apogee of the orbit and raise the perigee to the right altitude. Soon after, it will adjust the apogee from 35786 Km to 35790 Km and will head for the rendez-vous and subsequent deorbit of Hipparcos. Finished the first mission the chaser will move to ISO orbit changing inclination from 7,2° to 5,2° and shape, raising perigee and apogee, and finally deorbit ISO. To end the mission the chaser will rotate the orbit from 5,2° to 0° and circularize to GEO.

	Maneuver to...	ΔV $[\frac{m}{s}]$
Reach Hipparcos	Change inclination	34,078825
	Change chaser perigee	3,8889483
	Change chaser apogee	0,066369
Deorbit Hipparcos	Deorbit Hipparcos	7,334975
Reach ISO	Reach ISO (inclination + shape)	387,59099
	Secure chaser	8,4313387
Deorbit ISO	Drop ISO	2,9500425
Reach GEO	Change inclination	81,624374
	Change shape to GEO	1815,1205

Table 3.1: Hipparcos−ISO−GEO ΔV for each manoeuvre

Maneuver to...	Mass consumed $[Kg]$	Duration $[s]$
Change inclination Change chaser perigee Change chaser apogee	15,612422	122,86721
Deorbit Hipparcos	5,6191942	44,222141
Reach ISO (inclinaison + shape)	147,74561	1162,7338
Secure chaser	3,4204343	26,918259
Drop ISO	3,3745464	26,557129
Change inclination Change shape to GEO	508,80137	4004,1837

Table 3.2: Hipparcos−ISO−GEO mass consumed and duration of each impulse

The first 3 and the last 2 maneuvers have been grouped because they are performed in the same moment. This particular mission is the only which ends in GEO, in a future commercial servicing perspective.
The second mission evaluate the cost of Galileo reorbiting and ERS-1 deorbiting. Starting from the GTO the chaser will carry out an inclination change from 6° to 49,8° and then reach Galileo orbit. For Galileo cases, the cost of reorbiting is not considered, because the actual orbit to be reached is unknown. After Galileo it will perform inclination change to reach ERS-1's (98,5°), then adjust the shape to a LEO SSO and finally deorbit with ERS-1.
The third case follows the same structure of the previous one except for the aerobraking maneuver; comparison between the two cases, in fact, allows estimating the impact of aerobraking, in order to asses if it would have been worthwhile to perform despite the related difficulties

	Maneuver to...	ΔV $[\frac{m}{s}]$	Mass consumed $[kg]$
Reorbit Galileo	Change inclination	412,69748	650,49815
	Change orbit	775,36755	1478,6382
Reach ERS-1	Change inclination	1656,4963	552,44711
	Change shape	3395,8095	2620,6787
Deorbit ERS-1	Deorbit ERS-1	193,232	174,90622

Table 3.3: Galileo−ERS-1 ΔV and mass consumption during each boost

Maneuver to...	Duration $[s]$
Change inclination	5119,3141
Change orbit	11636,641
Change inclination	4347,6685
Change shape	20624,313
Deorbit ERS-1	1376,4834

Table 3.4: Duration of the impulse for each boost

	Maneuver to...	ΔV $[\frac{m}{s}]$	Mass consumed $[Kg]$
Reorbit Galileo	Change inclination	412,69748	410,38396
	Change orbit	775,36755	932,83801
Reach ERS-1	Change inclination	1604,0816	567,22319
	Reach aerobreaking orbit	1456,7318	836,03472
	Aerobraking (no consumption)		
	Raise perigee to ERS-1 orbit	149,2483	39,522359
Deorbit ERS-1	Deorbit ERS-1	193,232	175,8743

Table 3.5: Galileo−ERS-1 with aerobraking ΔV and mass consumption during each boost

Maneuver to...	Duration $[s]$
Change inclination	3229,6547
Change orbit	7341,2828
Change inclination	4463,9538
Reach aerobreaking orbit	6579,4567
Aerobraking (no consuption)	
Raise perigee to ERS-1 orbit	311,03451
Deorbit ERS-1	1384,102

Table 3.6: Duration of the impulse for each boost

The first thing that could be extracted from the comparison between 3.3 and 3.5 is the different consumed mass and duration of the impulse, which are considerably lower when aerobraking is performed and relates to a lower total mass of the spacecraft.
The last two cases regard deorbiting Hipparcos and ERS-1, with and without aerobraking. Both starts from the GTO, in which the chaser will perform an inclination change to reach Hipparcos', then adjust the orbit raising perigee and apogee and finally deorbit Hipparcos. To reach ERS-1 in both cases an inclination change from 7,2° to 98,5°, is carried out, after that the two cases split, in the first shape from GTO to LEO SSO is changed, in the second the perigee is lowered to aerobraking altitude and, once finished, circularized to LEO SSO; in the end ERS-1 is deorbited with the chaser.

	Maneuver to...	ΔV $[\frac{m}{s}]$	Mass consumed $[Kg]$
Reach Hipparcos	Change inclination	34,078825	40,865546
	Change chaser perigee	3,8889483	4,6916091
	Change chaser apogee	0,066369	0,0791554
Deorbit Hipparcos	Deorbit Hipparcos	7,334975	11,367764
Reach ERS-1	Change inclination	2261,6036	872,30658
	Change shape	2480,6442	2040,8946
Deorbit ERS-1	Deorbit ERS-1	193,232	176,81482

Table 3.7: Hipparcos−ERS-1 ΔV and mass consumed for each manoeuvre

Maneuver to...	Duration $[s]$
Change inclination	321,60517
Change chaser perigee	36,922197
Change chaser apogee	0,6229398
Deorbit Hipparcos	89,462446
Change inclination	6864,9103
Change shape	16061,507
Deorbit ERS-1	1391,5037

Table 3.8: Hipparcos−ERS-1 ΔV and mass consumed for each manoeuvre

	Maneuver to...	ΔV $[\frac{m}{s}]$	Mass consummed $[Kg]$
Reach Hipparcos	Change inclination	34,078825	18,281955
	Change chaser perigee	3,8889483	2,0988778
	Change chaser apogee	0,066369	0,0354116
Deorbit Hipparcos	Deorbit Hipparcos	7,334975	6,5389654
Reach ERS-1	Change inclination	2261,6036	853,10071
	Reach aerobraking orbit	15,881231	8,4192031
	Aerobraking(no comsuption)		
	Raise perigee to ERS-1 orbit	149,2483	37,577764
Deorbit ERS-1	Deorbit ERS-1	193,232	170,77498

Table 3.9: Hipparcos−ERS-1 ΔV and mass consumed for each manoeuvre with aerobraking

Maneuver to...	Duration $[s]$
Change inclination	143,876
Change chaser perigee	16,517825
Change chaser apogee	0,2786836
Deorbit Hipparcos	51,460589
Change inclination	6713,7632
Reach aerobraking orbit	66,257753
Aerobraking(no comsuption)	
Raise perigee to ERS-1 orbit	295,73086
Deorbit ERS-1	1343,9712

Table 3.10: Hipparcos−ERS-1 ΔV and mass consumed for each manoeuvre

Again as in 3.3 and 3.5 cases cruising between two targets, exploiting aerobraking to reduce the apogee, brings a noticeable saving in propellant mass, even if the most expensive ΔV, the inclination change to SSO, is carried out using chemical thrust.
To help the comparison and the subsequent choice of the best scenario, the results obtained above are reported in the following figures and Tables, in which they are split in accordance to the target to capture.

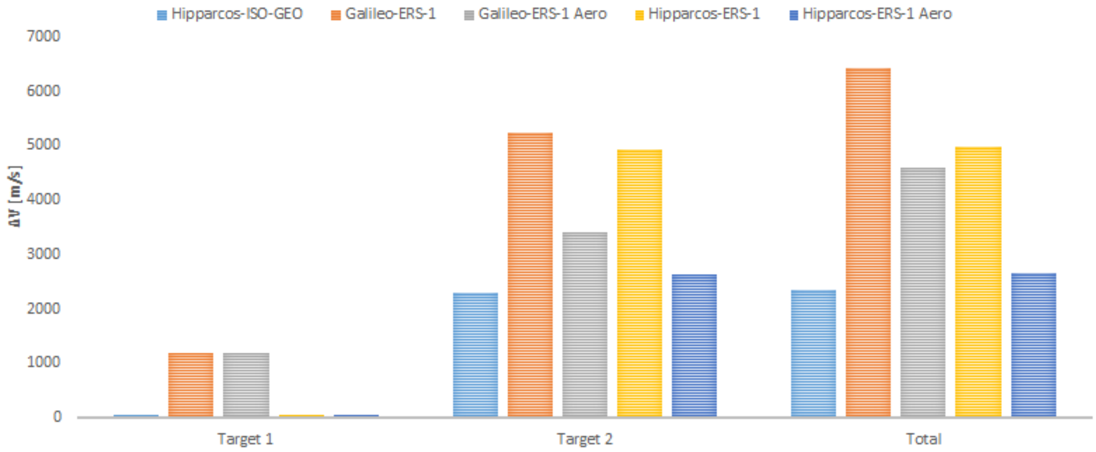

Figure 3.1: ΔV for each target and scenario

ΔV $[\frac{m}{s}]$	Target 1	Target 2	Total
Hipparcos−ISO−GEO	45,3691173	2295,7172	2341,08636
Galileo−ERS-1	1188,06503	5245,5378	6433,60283
Galileo−ERS-1 Aero	1188,06503	3403,2937	4591,35873
Hipparcos−ERS-1	45,3691173	4935,4798	4980,84892
Hipparcos−ERS-1 Aero	45,3691173	2619,9651	2665,33425

Table 3.11: Values of ΔV in fig.:3.1

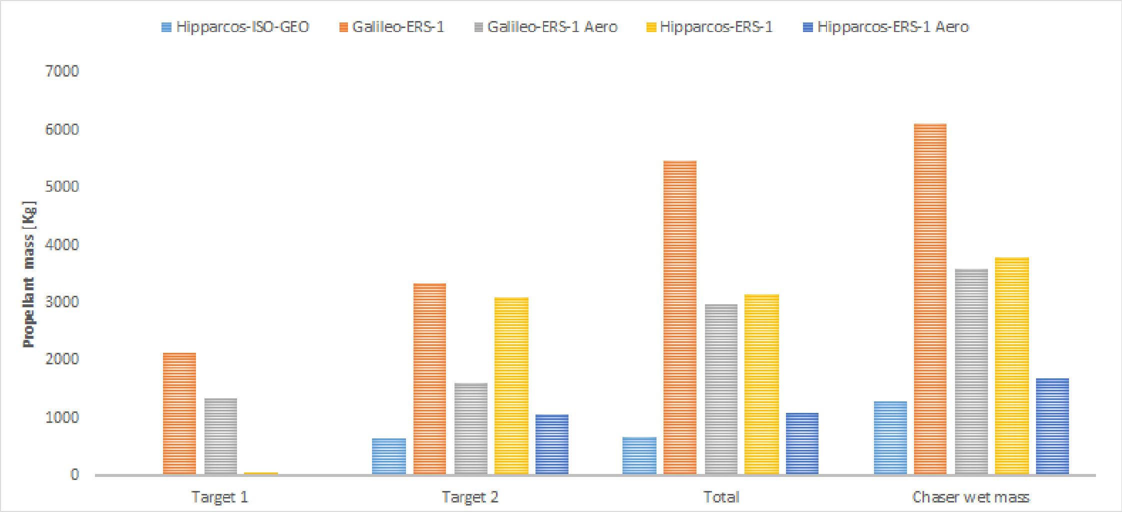

Figure 3.2: m_{prop} and m_{chaser} necessary for each mission

m_{prop} $[Kg]$	Target 1	Target 2	Total	Chaser wet mass
Hipparcos-ISO-GEO	21,2316162	663,341961	684,573577	1300
Galileo-ERS-1	2129,13635	3348,03203	5477,16838	6100
Galileo-ERS-1 Aero	1343,22197	1618,65457	2961,87654	3600
Hipparcos-ERS-1	57,0040745	3090,016	3147,02007	3800
Hipparcos-ERS-1 Aero	26,9552098	1069,87266	1096,82787	1700

Table 3.12: Values of m_{prop} and m_{chaser} in fig.:3.2

As shown by the Tables and figures above, reorbiting Galileo has a remarkable impact on the whole mission, not only because its orbit is expensive to reach from launcher's GTO, but also because the cost of reorbiting has to be considered in addition to the cost of the whole mission, making Galileo an unsuitable choice as first target. Moreover, Hipparcos is located on a GTO, which provides long exposure times in sunlight, thus simplifying rendez-vous and capture operations.
Hipparcos, on the contrary, seems to be the best choice as first target to deorbit, mainly because the launcher leaves the chaser satellite into a GTO very similar to Hipparcos', as can be seen in Table 2.1, reducing the cost of the whole mission both in terms of time and ΔV.
In this cases the $50\frac{m}{s}$ for the rendez-vous, are not considered for the trade-off because it is irrelevant for the ΔV budget. Anyway this cost will be counted in further results for a more accurate study.

3.2 IOS results

The selected missions are Hipparcos-ISO-GEO and Hipparcos-ERS-1 with Aerobraking due to their low cost in terms of ΔV and mass. Two different scenarios are selected to show flexibility, for future optimizations, to IOS approach. In order to improve their feasibility, both the deorbit of ISO and ERS-1 are removed and the chaser is supposed to carry a deorbiting/life extension kit to GEO or LEO SSO to service commercial satellites, or in the second case, possibly to deorbit ERS-1. To add more value to IOS outcomes refueling is introduced, which, if performed successfully, would represent a huge innovation for a more efficient usage of commercial satellites. Therefore it became necessary to replace Bi-prop with Hydrazine, due to TRL necessary for refueling, which led to an increase of the whole mission costs. To reduce them, is proposed the abovementioned hybrid propulsion system, which helped but brought complexity to the system.

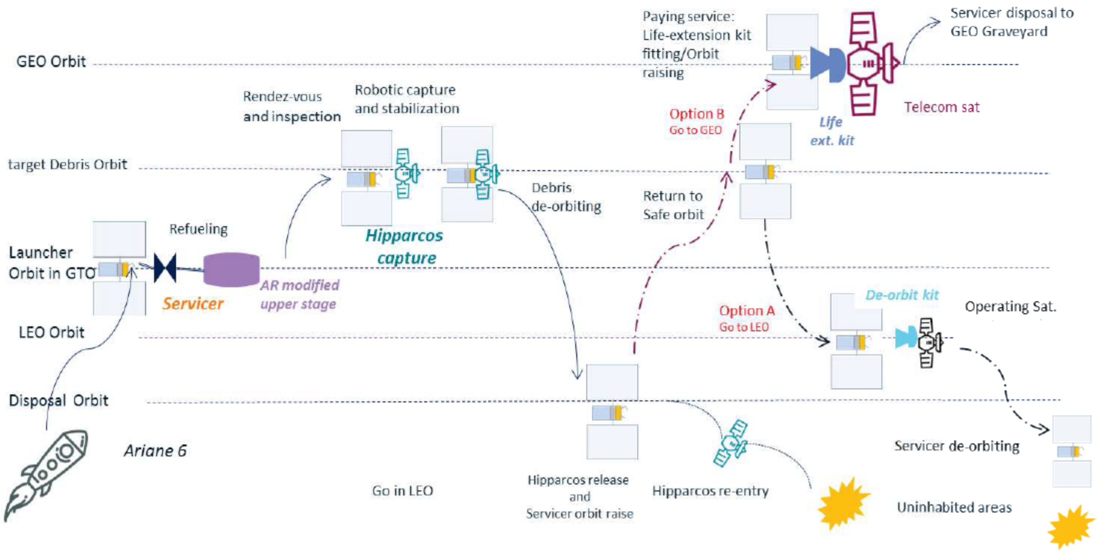

Figure 3.3: Pictorial view of the missions- courtesy of TAS

Reliable results are obtained introducing some scaling factors in the measures of the ΔV, in order to have a more robust sizing, due to the simplifications applied. These factors are: $1.3 \times \Delta V$ in case of inclination changes, $1.2 \times \Delta V$ for the other boosts; these are applied only to electric propulsion due to its continuous thrust which is more influencedby gravity effects. The peculiar hybrid propulsion system proposed is intended to use the electrical propulsion for maneuvers who requires high ΔV, while chemical thrusters are used when precision maneuvers occur like rendez vous or in case of low ΔV to save time.

In the end the final propellant mass is increased by 30% so that $m_f \neq m_{dry}$.

$$\begin{aligned} m_f &= m_{dry} + 0.3 m_{prop} \\ m_{prop} + m_{dry} &\leqslant m_i \end{aligned} \tag{3.2}$$

This increase is introduced to leave margin for late mission replanning, which in the preliminary analysis is not considered. In fact, in Hipparcos-ISO-GEO (see Tables 3.1 and 3.2)), once reached the GEO orbit the chaser hadn't enough propellant to perform any other operation.
Several parameters differ from the preliminary analysis; to have a better picture of the whole IOS missions, all the fixed parameters are reported in the Table below:

Chaser dry mass	700 Kg		I_{sp} $[s]$	Thrust $[N]$
Hipparcos mass	1130 Kg	Hydrazine	225	4×20
ERS-1 mass	2140 Kg	Xenon	1938	224×10^{-3}

Table 3.13: Reference parameters

For each of the selected cases, once released into the GTO, the chaser will immediately perform the refueling with the upper stage of Ariane 6, then it will change inclination to 7,2° and modify the orbit to reach Hipparcos'. After rendez-vous and deorbit of Hipparcos, in the first case the chaser will change inclination from GTO to GEO and then circularize the orbit. Once found a target and serviced, it will transfer itself into a graveyard orbit. In the second case, the chaser will change inclination to LEO SSO and exploits aerobraking to lower the apogee to 791 km. Adjusted the orbit, raising perigee altitude, it will identify a target, service it and perform a reentry in Earth atmosphere. All the maneuvers performed to reach Hipparcos use chemical propellant, while the second part of the mission use electric thruster when possible.
Follwing the Tables containing the results

Maneuver to...	Mass consumed $[Kg]$	Duration $[s]$
Reach AR6 upper stage	23,96583626	668,75
Change inclination	15,7814443	438,7379011
Change chaser perigee	11,4080646	316,5112608
Change chaser apogee	0,030634827	0,845246723
Deorbit Hipparcos and RDV	86,21542816	2427,773913
Change inclination (el. prop.)	10,58761925	$8{,}99 \times 10^5$
Raise perigee to GEO altitude (el. prop.)	86,6389107	$7{,}35 \times 10^6$
Rendez-vous of target in GEO	18,7106449	522,1075387
Chaser reach graveyard orbit (el. prop.)	0,587011241	49822,00253

Table 3.15: Hipparcos−GEO propellant consumed and duration for each boost

	Maneuver to…	ΔV $[\frac{m}{s}]$
In GTO	Reach AR6 upper stage	50
Reach Hipparcos	Change inclination	33,55544
	Change chaser perigee	24,5774
	Change chaser apogee	0,066369
Deorbit Hipparcos	Deorbit Hipparcos and RDV	90,3856
Reach GEO	Change inclination (el. prop.)	167,6983
	Raise perigee to GEO altitude (el. prop.)	1488,739
	Rendez-vous of target in GEO	50
Chaser disposal	Chaser reach graveyard orbit (el. prop.)	11,388

Table 3.14: Hipparcos−GEO ΔV necessary for each boost

	Maneuver to...	ΔV $[\frac{m}{s}]$
In GTO	Reach AR6 upper stage	50
Reach Hipparcos	Change inclination	33,55544
	Change chaser perigee	24,5774
	Change chaser apogee	0,066369
Deorbit Hipparcos	Deorbit Hipparcos and RDV	90,3856
Reach LEO (ESR-1 orbit)	Change inclination (el. prop.)	2291,646
	Aerobraking (no consumption)	
	Raise perigee to LEO altitude (el. prop.)	147,6221
	Rendez-vous of target in LEO	50
Chaser disposal	Deorbit chaser (el. prop.)	197,1812

Table 3.16: Hipparcos−LEO ΔV necessary for each boost

Maneuver to...	Mass consummed (kg)	Duration (s)
Reach AR6 upper stage	27,32553293	762,5
Change inclination	17,99379631	500,2432144
Change chaser perigee	13,00732599	360,8819982
Change chaser apogee	0,034929429	0,963739254
Deorbit Hipparcos and RDV	91,94587587	2589,139828
Change inclination (el. prop.)	167,6171431	$1{,}42 \times 10^7$
Aerobraking (no consumption)		TBD
Raise perigee to LEO altitude (el. prop.)	8,405288345	713390,5931
Rendez-vous of target in LEO	20,01640325	558,5438175
Deorbit chaser (el. prop.)	10,87334811	922864,7417

Table 3.17: Hipparcos−LEO propellant consumed and duration for each boost

	RDV Upper stage	Mission 1	Mission 2	Total
ΔV $[\frac{m}{s}]$	50	148,5848	1717,8248	1916,4096
Xenon propellant			1667,8248	1667,8248
Hydrazine propellant	50	148,5848	50	248,5848
Mass consummed $[Kg]$	23,9658	113,4314	116,5241861	253,9214
Xenon propellant			97,8135	97,8135
Hydrazine propellant	23,9658	113,4355	18,7106	156,1120
Duration $[s]$	668,75	3183,8683	8302350	8306871
Xenon propellant			8301828	8301828
Hydrazine propellant	668,75	3183,8683	522	4374

Table 3.18: Hipparcos-GEO total values of ΔV, mass consumed and duration of each boost, divided between the two types of propellants

	RDV Upper stage	Mission 1	Mission 2	Total
ΔV $[\frac{m}{s}]$	50	148,5848	2686,4497	2885,0345
Xenon propellant			2636,4497	2636,4497
Hydrazine propellant	50	148,5848	50	248,5848
Mass consummed $[Kg]$	27,3255	122,9819	206,9121	357,2195
Xenon propellant			186,8957	186,8957
Hydrazine propellant	27,3255	122,9819	20,0164	170,3238
Duration $[s]$	762,5	3451,2287	15863154	15867367
Xenon propellant			15862595	15862595
Hydrazine propellant	762,5	3451,2287	558	4772

Table 3.19: Hipparcos-LEO total values of ΔV, mass consumed and duration of each boost, divided between the two types of propellants

	Hipparcos-GEO	Hipparcos-LEO
Chaser initial mass $[Kg]$	1070	1220
Chase final mass $[Kg]$	816	860

Table 3.20: Mass values of the chaser for the two cases

As it possible to see from table 3.19 and 3.20 using electric propulsion and aerobraking reduce significantly the mass of the whole system with respect to only chemical propulsion. This 2 cases are selected to answer the RFI due to the their relative easiness for performing deorbiting and refuelling. The only remaining issue are the current dynamics of Hipparcos, which is unknown and could prevent the capture by robotic means. Therefore are identified other targets to remove, that have similar orbital parameters to Hipparcos' and could be easily reached from AR6 GTO, which are Sloshat-FLEVO,MaqSat-H and Cat4. These targets despite being unoperative since few days after the launch, are smaller and at least one could be cooperative with the chaser. The technologies developed for these services in the future will acquire a key role, both for commercial and scientific purposes, in reducing the costs for space missions and providing a sustainable approach to the space environment, which, surrounding the Earth, has a significant impact on our lives, directly and indirectly.

Chapter 4

Robotics introduction

4.1 A Review On Space Manipulators

Spacecraft mounted robotic arms represent next generation of commercial space mission, from in orbit servicing to active debris removal or asteroid mining, thanks to their capability in performing very different tasks, without endangering astronauts safety, that otherwise could be forced to do EVAs (Extra-Vehicular activity).
Spacecraft-mounted robotic manipulators have a successful history in Space Shuttle and International Space Station programs. STS-3 was the first mission to use a manipulator in space, known as Shuttle Remote Manipulator System (SRMS) or Canadarm, and since then it was used for various tasks, to capture Hubble Space Telescope for servicing, to position astronauts during extra-vehicular activities or to assemble and resupply the ISS. The ISS too is equipped with robotic manipulators, the Space Station Remote Manipulator System or Canadarm 2 [2] and Japanese Experiment Module Remote Manipulator System [3].
Canadarm 2 is used to capture and berth H-II Transfer Vehicle (HTV), Dragon, and Cygnus vehicles as well as to position astronauts and equipment ([4], [5], [6]); at its end is mounted the Special Purpose Dexterous Manipulator (also called Dextre) as grappling system, which is capable of fine manipulation like refuelling of a satellite, through accessing and operating on the fuel port, as in NASA Robotic Refuelling Mission. Japanese robotic arm, on the other side, is mostly used to service the Japanese Experiment Module "Kibo", even if it is also equipped with a dexterous end effector.
Space manipulators were not only mounted on big spacecraft, but also on small ones for servicing and refuelling of client satellites, like has been demonstrated in Engineering Test Satellite VII (ETS-VII) [7] mission and Orbital Express [**?**], in which the robotic arm was controlled both remotely or autonomously by the ASTRO mission manager software. Further servicing demonstration missions were proposed, to exploit the advantages of robotic manipulators for capture and servicing, like the U.S. upcoming mission Restore-L and Robotic Servicing of Geosynchronous

Satellites (RSGS).
Operating a robotic manipulator in space represents a relevant challenge because it involves two different disciplines such as Robotics and Aerospace Engineering. The dynamics of the manipulator are coupled with the base, therefore an integrated control system is required to capture and operate on the target safely. The Space Shuttle Orbiter and the ISS are less sensitive to the coupling effects, due to their big mass and inertia with respect to the arm; the disturbances in position and orientation could be easily managed through operational procedures. For small and fast moving satellites, like ETS-VII and Orbital Express have shown, coupling effects became relevant and the disturbances in position and orientation must be controlled carefully to reach manipulator goals and grant mission success.

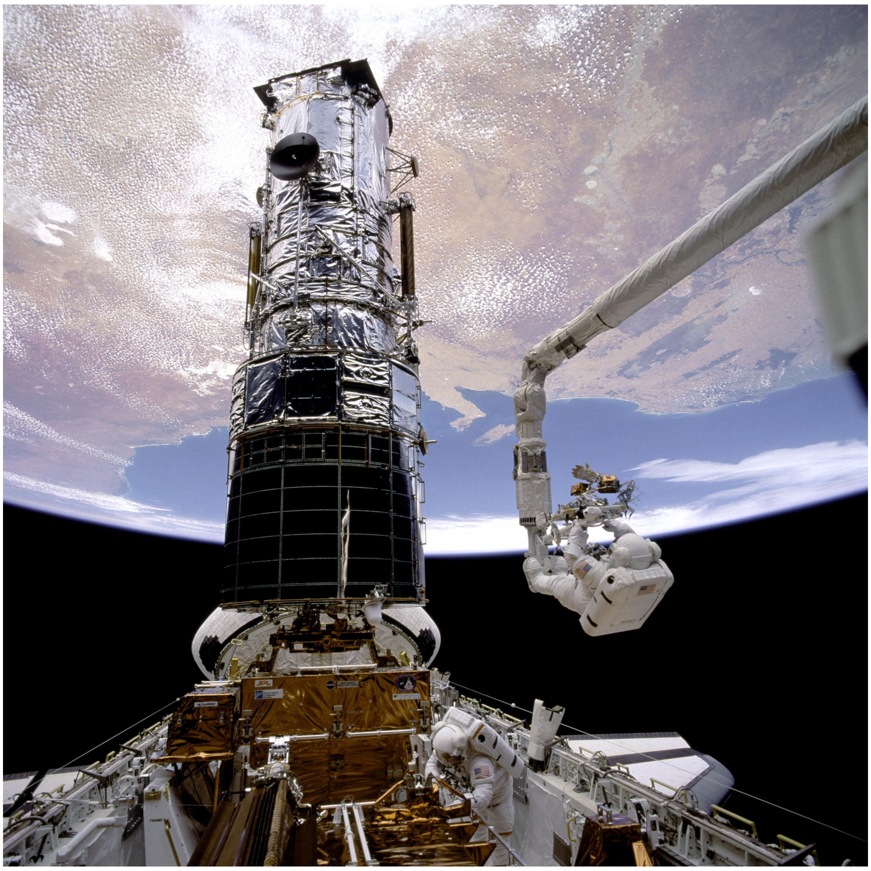

Figure 4.1: Canadarm carring an astronaut to Hubble Telescope for servicing during STS-61

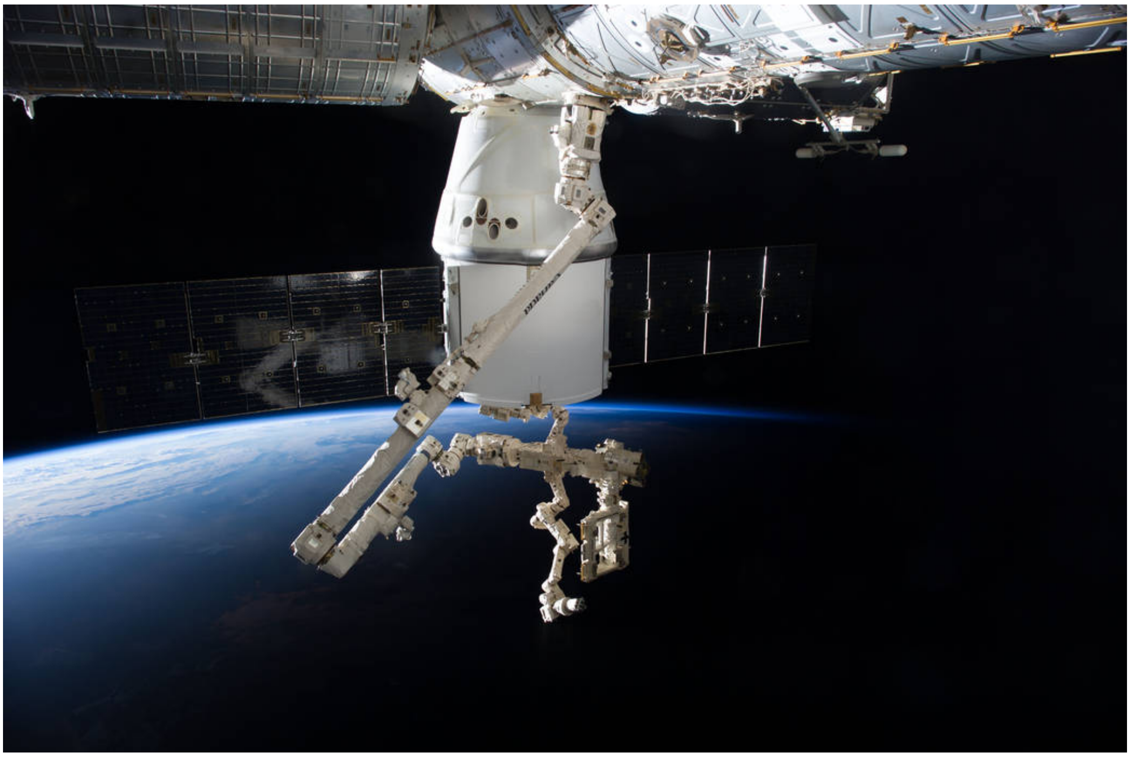

Figure 4.2: Canadarm 2 using Dextre to remove external cargo from Dragon cargo ship

4.2 Operational Use

In this context TAS has started a study that includes the design of a space robotic arm and its modeling for simulation purposes. The arm once mounted on a spacecraft would capture and operate on target satellites. The manipulator used as reference for the thesis, designed only at an early stage, will be a 7 D.o.F. (Degrees of Freedom) arm, to have D.o.F. redundancy exploitable for avoiding kinematics singularities; on the elbow of the arm will be mounted two cameras, in case one is not enough, for determinating target pose, while on the end effector one more camera will be mounted to identify precisely the position of the point to grasp with respect to the chaser. The manipulator becomes operational in the final phase of rendez-vous when the relative motion between the chaser and the target is limited only to attitude. The whole capture phase can be divided in 6 subphases, to have a clearer vision of the sequential actions to be performed for fulfilling the capture. Below each phase is specified in order of execution, starting from deployment to grasping

1. **Target Search**
   The cameras mounted on the chaser should find the target spacecraft and

obtain information about its pose with respect to the chaser.

2. **Manipulator Deployment**
   Starting from stowed configuration, the arm is deployed, through direct kinematics control, in a safe position, carefully selected to not obscure the cameras field of view and to avoid catastrophic collision with the target.

3. **Approach To Target**
   Once obtained the target pose, it is possible to command the End Effector to move towards a specific point on its surface, through inverse kynematics, and stop at a certain distance(0,5 m).

4. **Grasping Point Search**
   The camera located on the end effector will search, through an image processing algorithm, a suitable grasping point on the target, to identify its pose with respect to the chaser.

5. **Approach To Grasping Point**
   After the information about the target are obtained, is possible to move very closely towards the grasping point ($5cm$), through inverse kynematics control.

6. **Grasping Of The Target**
   Once close to the target, the manipulator is commanded to capture it, through a force control algorithm (Impedance Control) able to manage the occurring contact forces; if secured the end effector must send a feedback signal.

As mentioned above, there are three different control modes, depending on the operation to perform:

1. Direct Kinematics: the actuator of each joint is commanded to rotate to a desired angle.

2. Inverse Kinematics: Based on the desired position and orientation of the End-Effector, the angle by which each joint has to rotate is computed .

3. Impedance Control: The actuators are commanded to apply a torque, basing on the forces and torques acting on the End-Effector and the and the current state of the manipulator.

4.3 Dynamics Modeling

Modelling of the manipulator used in TAS study has been performed starting from a model of a standard ground based manipulator developed by an external company during the initial phase of the study. This paragraph summarizes the

methods available for manipulator modeling and highlights the problems associated with the integration of the model of a ground based manipulator in the model of a free flying manipulator. There are various methods for modeling the dynamics of a manipulator, but the most common are the Lagrangian and Newton-Euler recursive method [15].
Newton-Euler formulation is based on the balance of all forces and torques acting on a single link of the manipulator. This leads to develop a set of equations whose structure allows a recursive algorithm through the multibody system. Forward recursion is used to obtain both angular and linear velocities and acceleration, while through backward recursion are computed forces and moments acting on the various body of the system. In case of flexible links, the Direct Path Method was developed, in which the equations of motion are computed with respect to the center-of-mass of the base instead of the center-of-mass of the whole system and the structure of the system is described following the most direct path.

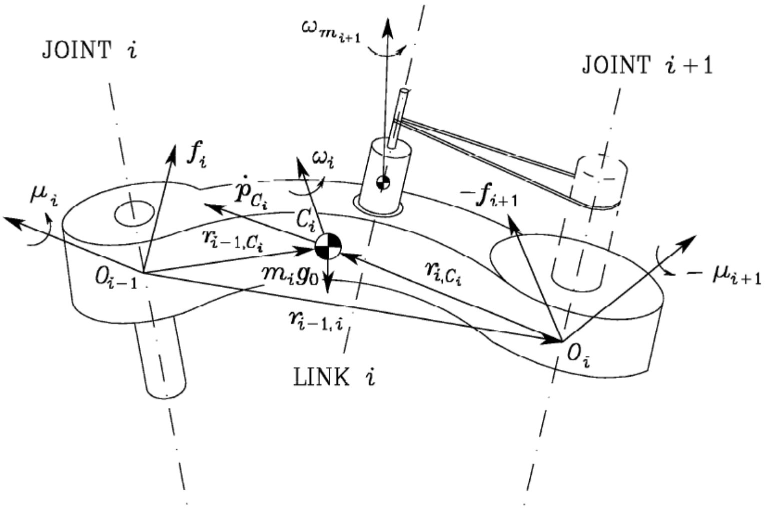

Figure 4.3: Link characterization for Newton-Euler formulation

Lagrangian formulation on the other hand develops the equations of motion from the kinetic and potential energy of the system, independently of the reference frame. To describe effectively the position of the links is used a set of variables, termed generalized coordinates, like the joint rotational angles $q_i\, i = 1, ..., n$, through which it is possible to define the Lagrangian of the whole mechanical system:

$$\mathcal{L} = \mathcal{T} - \mathcal{U} \tag{4.1}$$

in which $\mathcal{T}$ and $\mathcal{U}$ represent kinetic and potential energy and the Lagrange equations could be expressed as:

$$\frac{d}{dt}\frac{\partial \mathcal{L}}{\partial \dot{q}_i} - \frac{\partial \mathcal{L}}{\partial q_i} = \xi_i \tag{4.2}$$

in which ξ_i represent the generalized force associated with the generalized coordinate q_i. Once the Lagrange equations are made explicit, the equations of motion are obtained.
Newton-Euler formulation due to its recursive nature is computationally more efficient than Lagrange's, yet it remains conceptually less simple. The latter, due to its being systematic, is more suitable for control system design.
The manipulator model was provided by Graaltech s.r.l., an external company with over 15 years of experience in mechatronics solutions in water and underwater environement. The manipulator was intended for ground based operations, thus was necessary to implement base dynamics and dynamic coupling between the base and the robotic arm to simulate a complete spacecraft. The main issue concerned the different algorithms used, because the model received was created following Newton-Euler formulation, while the equations used for obtaining dynamic coupling were written used Lagrangian formulation, as will be shown in the following chapter.
The system of equations to resolve is in the following form:

$$\begin{bmatrix} H_0 & H_{0m} \\ H_{0m}^T & H_m \end{bmatrix} \begin{Bmatrix} \ddot{x} \\ \ddot{q} \end{Bmatrix} + \begin{bmatrix} C_0 & C_{0m} \\ C_{m0} & C_m \end{bmatrix} \begin{Bmatrix} \dot{x} \\ \dot{q} \end{Bmatrix} + \begin{bmatrix} 0 & 0 \\ 0 & F_v \end{bmatrix} \begin{Bmatrix} \dot{x} \\ \dot{q} \end{Bmatrix} = \begin{bmatrix} 0 \\ \tau \end{bmatrix} \tag{4.3}$$

in which $x = [\omega_0 \; v_0]^T$ and q are the base and joint variables. H_b, H_m and H_{bm} are respectively: the inertia matrix of the base $[6 \times 6]$, the inertia matrix of the manipulator $[N \times N]$ (with N equal to the number of D.o.F) and the dynamic coupling inertia matrix $[6 \times N]$. The C matrices, called convective inertia matrix, represent the non linear contribution of the velocities to the dynamics, while F_v represents the viscous friction in the joints and τ are the torques acting on the joints.
The matrices, C_m and H_m, referred to the manipulator are already computed in the external model, while, for the remaining, different papers provided a formulation. Inertia matrices were the only which had explicit equations, convective matrices, on the other hand, due to their non-linearity, required the computation of multiple derivatives. For this reason it was performed a research between several papers, in order to find a practical way to compute them. During the reserach was found a MATLAB toolkit named SPART(SPAce Robotic Toolkit)[14], supported by various articles. SPART offered a tool capable of providing the missing matrices, but several issues occurred in integrating SPART with the model, again due to the different formulation used.

4.4 Model Description

Currently several softwares exist for modeling and simulating dynamic systems, such as Scilab or Simulink. The latter was chosen for the manipulator model, due to its practicality in creating, analysing and simulating dynamic systems. Simulink is closely linked to MATLAB and it allows to create and merge different dynamic models with relative ease and, thanks to its blocks structure, it also provides a quite immediate and intuitive view of the model displayed.
The whole structure of the Space Manipulator is built on the Graaltech Simulink manipulator model which provided a robust base to start from. The model keeps following Graaltech's and could be divided in 3 main susbsystem located one inside the other: the inner one, shown in fig 4.4 contains the computations necessary for evaluating all the matrices associated to eq. 4.3; the middle one, represented in fig 4.5, solves the dynamic equation 4.3 and evaluates the states variables and the velocities of the system; the outer, as in fig 4.6, contains the control system necessary to evaluate the control torques for the whole model and dynamic model of the spacecraft/manipulator.

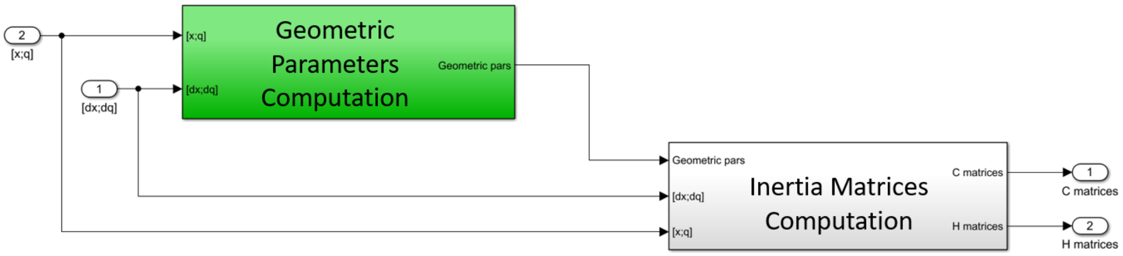

Figure 4.4: Inner susbsystem computing the position of each body wrt inertial frame and the inertia matrices associated to the system

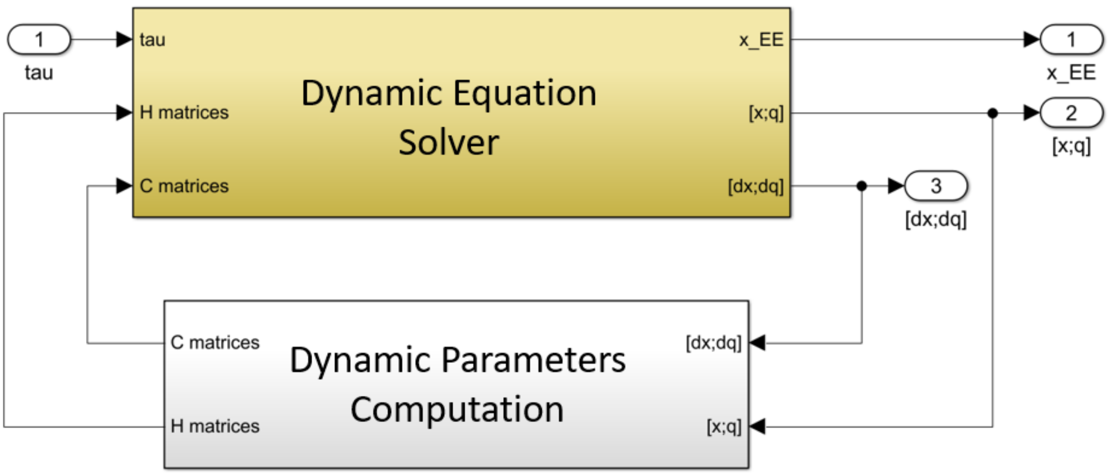

Figure 4.5: Middle susbsystem computing the state variables and the velocities of the system

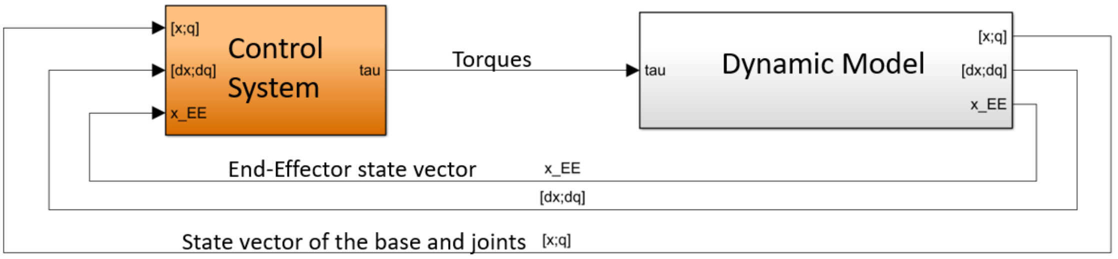

Figure 4.6: Outer subsystem computing the control torques of the system

Chapter 5

Robotics Equation

5.1 Geometric characterization

Lagrange and Newton-Euler formulations despite their different approaches to robot dynamics, share common geometric chain of the model, which helped in integrating the methods. The initial configuration of the manipulator was assessed by a set of parameters, called "Robot", which contained:

- N number of joints (D.o.F.), joints are designed from 1 ìto N, while for $i = 0$ is intended the base-spacecraft and with $i = N + 1$ is intended the End-Effector.

- alf $[m]$ distance between the ith joint frame and $(i + 1)th$ expressed in the ith joint frame, when $i = N$ is the distance between the last joint and the end effector.

- alc $[m]$ distance between the ith joint frame and the center-of-mas of the ith body, expressed in the ith joint frame. When $i = N$ represents the distance between the last joint frame and the last center-of-mass including last link and end effector.

- am $[Kg]$ is the mass of the ith body, when $i = N$ is the mass of the last link, including the end effector.

- ai is the $[3 \times 3]$ inertia matrix of the ith link body, expressed with respect to a frame oriented as the ith joint frame, but translated in ith body center-of-mass. When $i = N$ is the resulting inertia from last link and End-Effector.

- $arot$ is the $[3 \times 3]$ rotation matrix transforming points expressed in ith frame of the kinematic chain, into $(i - 1)th$ frame of the kinematic chain, when ith joint angle is $0\,rad$. When $i = 1$, it is the rotation matrix from first joint frame to Base frame, when first joint angle is $0\,rad$.

- jlf $[m]$ is the vector connecting Base frame with first joint frame, expressed in Base frame.

- bi is the $[3 \times 3]$ inertia matrix of the Base body, expressed with respect to a frame oriented as the Base frame, but translated in the Base COM.

- bm $[kg]$ is the mass of the Base body.

- $hrot$ is the $[3 \times 3]$ rotation matrix transforming points from End-Effector frame to last joint frame.

- blf $[m]$ is the vector connecting Inertial frame with Base frame, expressed in Inertial frame.

- $brot$ is the $[3 \times 3]$ rotation matrix transforming points from Base frame to inertial frame when the base orientation is $[0, 0, 0]$.

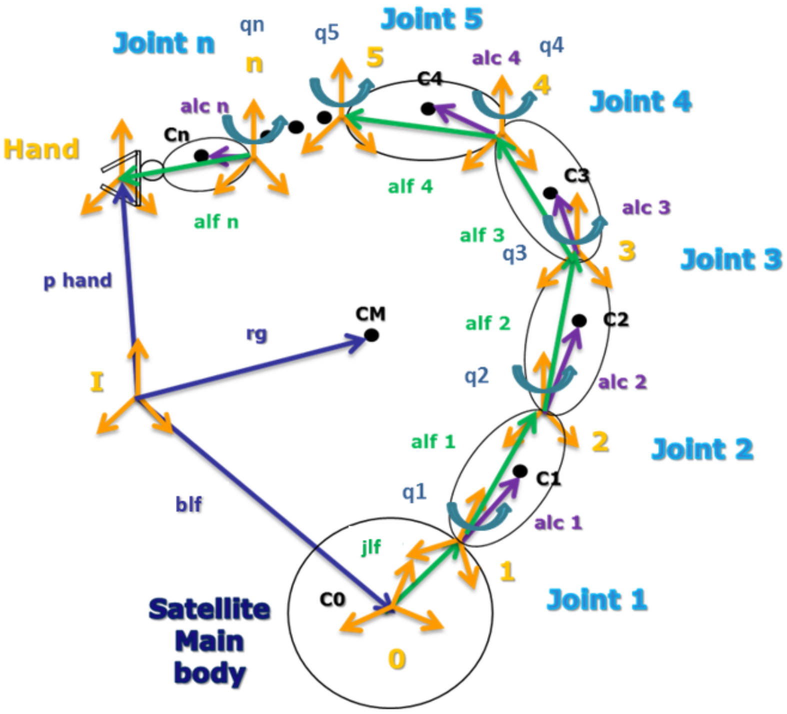

Figure 5.1: Geometric model of a space manipulator

Once defined all these parameters, to completely characterize the initial configuration it is necessary to specify the initial condition of the joints and the base, which temporarily could be set as $x = [0\,0\,0\,0\,0\,0]$ and $q = [0\,0\,0\,0\,0\,0\,0]$. In particular the

base state vector is divided into angular and linear component, such as the base velocity results: $\dot{x} = [\omega_0 \;\; v_0]$.
For comprehensibility purposes, to have a unified notation between the external model, SPART and the paper, the notation regarding the various distances will change, soon after are applied equations 5.4, according to the following image.

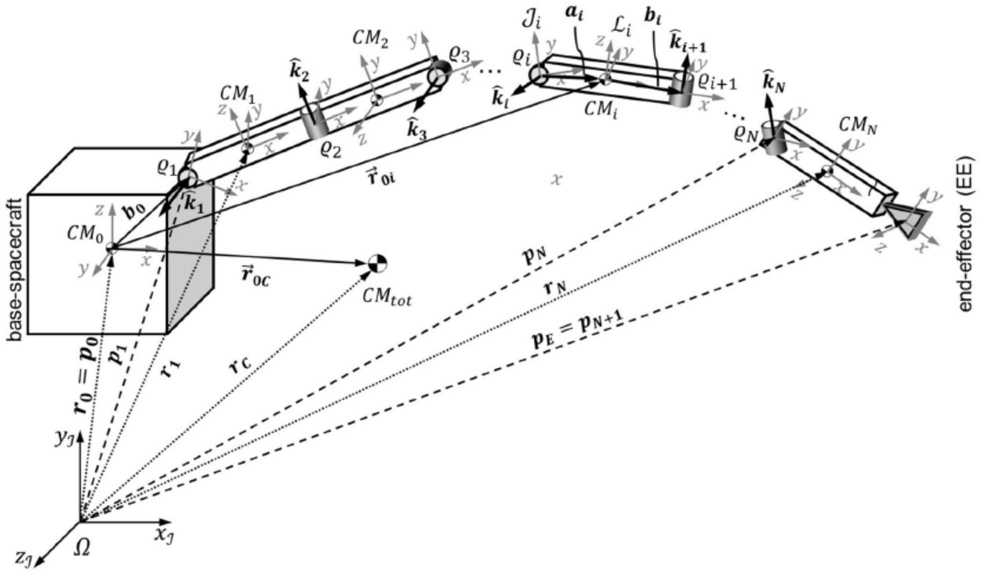

Figure 5.2: Geometric model of a space manipulator

According to fig 5.2 the renamed variables are:

- $a_i = alc_i$
- $ab_i = alf_i$
- $b_i = alf_i - alc_i$ represent the distance between ith link center-of-mass and the origin of $(i+1)th$ joint frame.
- r_i represents the distance between the origin of the inertial frame and the center-of-mass of the ith link.
- p_i represents the distance between the origin of the inertial frame and the origin of ith joint frame.
- $blf = r_0$

To define the whole geometric configuration it is necessary to express every variable in the inertial reference frame. First of all each $arot$ must be updated to the current angle of the related joint, so:

$$^{i-1}R_i = arot \times R_{q_i} \tag{5.1}$$

with

$$R_{q_i} = \begin{bmatrix} \cos\psi & -\sin\psi & 0 \\ \sin\psi & \cos\psi & 0 \\ 0 & 0 & 1 \end{bmatrix} \tag{5.2}$$

in which R_{q_i} is the rotation matrix associated to *ith* joint considering only a rotation around its z axis. Then, the same logic is applied to the base, but to avoid errors from Gimbal Locking, are used quaternion instead of Euler angles to update *brot*, following the transformation: from the first three values of x is computed the initial quaternion, through a 1-2-3 rotation sequence, and from the quaternion is obtained the rotation matrix with which update the *brot*.
Through a forward recursion is possible to express ${}^{\mathcal{I}}R_i$, sequentially multiplying each ${}^{i-1}R_i$ until the desired joint/link is reached

$${}^{\mathcal{I}}R_i = {}^{\mathcal{I}}R_0 {}^{0}R_1 .... {}^{i-2}R_{i-1} {}^{i-1}R_i \qquad i = 0....N+1 \tag{5.3}$$

Once obtained each ${}^{\mathcal{I}}R_i$, every "Robot" variable is reported to the inertial frame:

$$\begin{aligned} i &= 1....N \\ ab_i &= {}^{\mathcal{I}}R_i \, alf_i \\ a_i &= {}^{\mathcal{I}}R_i \, alc_i \\ I_i &= {}^{\mathcal{I}}R_i^T \, ai \, {}^{\mathcal{I}}R_i \\ b_0 &= {}^{\mathcal{I}}R_i \, jlf \\ \hat{k}_i &= {}^{\mathcal{I}}R_i \begin{bmatrix} 0 \\ 0 \\ 1 \end{bmatrix} \end{aligned} \tag{5.4}$$

Through a backward recursion are obtained the distances between each joint and the End-Effector and soon after are derived other distances useful for further computations

$$\begin{aligned} i &= N....1 \\ p_{i,EE} &= p_{i+1,EE} + ab_i \qquad (when \;\; i = N+1, \;\; p_{N+1,EE} = 0) \\ p_{0,EE} &= p_{1,EE} + b_0 \\ p_{\mathcal{I},EE} &= p_{0,EE} + blf \\ p_{0,i} &= p_{0,EE} - p_{i,EE} \\ r_{0,i} &= p_{0,EE} + b_i \end{aligned} \tag{5.5}$$

Once computed all the $r_{0,i}$, the center-of-mass of the whole system, with respect to base spacecraft, could be found starting from the relation:

$$\begin{aligned} r_{0,CM} &= \frac{m_{tot}}{\sum_{i=1}^{N} m_i r_{0,i}} \\ r_{CM} &= r_{0,CM} + blf \end{aligned} \tag{5.6}$$

After each time step the whole process is repeated, rotational matrices and r_0 are updated to current variables. While for the joints is always applicable equation 5.1 with the current angle, for the base must be used the quaternion propagation equation which involves base rotation angles $\phi\,\psi\,\theta$ and base angular velocity $\omega = [p\,q\,r]$:

$$q_t = \int_{t-1}^{t} \dot{q} \tag{5.7}$$

$$\dot{q} = \frac{1}{2}\Omega(\omega)q_{t-1} + \varepsilon q_{t-1} \tag{5.8}$$

$$\Omega = \begin{bmatrix} 0 & -p & -q & -r \\ p & 0 & r & -q \\ q & -r & 0 & p \\ r & q & -p & 0 \end{bmatrix} \tag{5.9}$$

$$\varepsilon = 1 - \left(q_0^2 + q_1^2 + q_2^2 + q_3^2\right)$$

where $\dot{q}$ is the quaternion derivative and ε is introduced to correct possible occurring errors during the integration phase.
The distance between base center-of-mass and inertial frame, on the other hand, is updated adding the displacement of the base, caused by the coupling with the manipulator:

$$r_0^t = r_0^{t-1} + x^t \tag{5.10}$$

where r_0^t is the position of the base at time t.
Ended this phase, Lagrangian and Newton-Euler formulations diverge from each other; Lagrangian is the former to be described, for two main reason: firstly because it was used to describe the dynamics of the whole model, while Newton-Euler was used only to compute the manipulator related matrices; secondly because, due to its systematic nature, outline the system dynamics clearly.

5.2 Lagrangian Formulation

The total energy of the system is expressed in eq 4.1, but in the considered case the potential energy is zero, therefore it becomes:

$$\mathcal{L} = \mathcal{T} = \frac{1}{2}\sum_{i=0}^{N}\left(\omega_i^T I_i \omega_i + m_i \dot{r}_i^t \dot{r}_i\right) \tag{5.11}$$

collecting all mass and inertia properties of the system and rearranging the equation, an explicit form of the kinetic energy is obtained [13]:

$$\begin{aligned} T &= \frac{1}{2}\left\{\dot{x}_0^T \quad \dot{q}^T\right\}\begin{bmatrix} H_0 & H_{0m} \\ H_{m0}^T & H_m \end{bmatrix}\begin{Bmatrix} \dot{x}_0 \\ \dot{q} \end{Bmatrix} \\ &= \frac{1}{2}\dot{x}_0^T H_0 \dot{x}_0 + \frac{1}{2}\dot{x}_0^T H_{0m}\dot{q} + \frac{1}{2}\dot{q}^T H_{0m}^T \dot{x}_0 + \frac{1}{2}\dot{q}^T H_m \dot{q} \end{aligned} \tag{5.12}$$

with $\dot{x} = [\omega_0 \ v_0]$.
Now is possible to apply the Lagrangian equation, as in 4.2, to derive equation 4.3 reported below:

$$\begin{bmatrix} H_0 & H_{0m} \\ H_{0m}^T & H_m \end{bmatrix}\begin{Bmatrix} \ddot{x} \\ \ddot{q} \end{Bmatrix} + \begin{bmatrix} C_0 & C_{0m} \\ C_{m0} & C_m \end{bmatrix}\begin{Bmatrix} \dot{x} \\ \dot{q} \end{Bmatrix} + \begin{bmatrix} 0 & 0 \\ 0 & F_v \end{bmatrix}\begin{Bmatrix} \dot{x} \\ \dot{q} \end{Bmatrix} = \begin{bmatrix} 0 \\ \tau \end{bmatrix} \tag{5.13}$$

in the equation above the matrices that govern the dynamics of a space manipulator are described. The inertia matrices H have an analytical formulation and are expressed below, starting from the [6 × 6] Inertia Base Matrix:

$$H_0 = \begin{bmatrix} m_{tot}\mathbb{I}_{3,3} & -m_{tot}r_{0,C}^{\times} \\ m_{tot}r_{0,C}^{\times} & H_S \end{bmatrix} \tag{5.14}$$

with

$$a^x = \begin{bmatrix} 0 & -a_3 & a_2 \\ a_3 & 0 & -a_1 \\ -a_2 & a_1 & 0 \end{bmatrix} \tag{5.15}$$

where $\mathbb{I}_{3,3}$ is the [3 × 3] identity matrix, while the [3 × 3] H_S matrix collects the inertia moments from both base-spacecraft and manipulator about the base-spacecraft center-of-mass, expressed in the inertial frame:

$$H_S = \sum_{i=1}^{N}\left(I_i - m_i r_{0,i}^{\times} r_{0,i}^{\times}\right) + I_0 \tag{5.16}$$

Then there is the [6 × N] Dynamic Coupling Inertia matrix, which expresses the contribution of the manipulator to the base dynamics and vice versa:

$$H_{0m} = \begin{bmatrix} J_{TS} \\ H_{Sq} \end{bmatrix} \tag{5.17}$$

in which the [3 × N] H_{Sq} submatrix collects the dynamic contribution to the system of the combined effects of the manipulator joint rates $\dot{q}$ and base-spacecraft angular velocity ω_0:

$$H_{sq} = \sum_{i=1}^{N}\left(I_i J_{Ri} + m_i r_{0,i}^{\times} J_{Ti}\right) \tag{5.18}$$

where

$$J_{Ti} = \left[\hat{k}_1^{\times}(r_i - p1), \hat{k}_2^{\times}(r_i - p2), \cdots, \hat{k}_i^{\times}(r_i - pi), 0_{3,N-i}\right] \quad \forall 1 \leq i \leq N \tag{5.19}$$

is a $[3 \times N]$ matrix that represents the linear velocity Jacobian for the center of mass of the *ith* link and J_{Ri} represents the angular velocity Jacobian for the *ith* link:

$$J_{Ri} = \left[\hat{k}_1, \cdots, \hat{k}_i, 0_{3,N-1}\right] \quad \forall 1 \leq i \leq N \tag{5.20}$$

The $[3 \times N]$ J_{TS} submatrix collects the dynamic contribution of the combined effects of the manipulator joint rates $\dot{q}$ and base-spacecraft linear velocity v_0:

$$J_{TS} = \sum_{i=1}^{N}(m_i J_{Ti}) \tag{5.21}$$

Finally the Manipulator Inertia matrix,H_m which is a $[N \times N]$ identical to any of a ground based manipulator:

$$H_m = \sum_{i=1}^{N}\left(J_{Ri}^T I_i J_{Ri} + m_i J_{Ti}^T J_{Ti}\right) \tag{5.22}$$

To express the C matrices, on the other hand, following Lagrangian procedure became necessary to solve the following derivatives [17]

$$\frac{d}{dt}\begin{bmatrix} H_0 & H_{0m} \\ H_{m0}^T & H_m \end{bmatrix} - \begin{bmatrix} c_0 \\ c_m \end{bmatrix} \tag{5.23}$$

having

$$c_0 = -\frac{\partial T}{\partial x_0} = -\frac{1}{2}\frac{\partial}{\partial x_0}\left(\dot{x}_0^T H_0 \dot{x}_0 + \dot{x}_0^T H_{0m}\dot{q} + \dot{q}^T H_{0m}^T \dot{x}_0 + \dot{q}^T H_m \dot{q}\right) \tag{5.24}$$

$$c_m = -\frac{\partial T}{\partial q} = -\frac{1}{2}\frac{\partial}{\partial q}\left(\dot{x}_0^T H_0 \dot{x}_0 + \dot{x}_0^T H_{0m}\dot{q} + \dot{q}^T H_{0m}^T \dot{x}_0 + \dot{q}^T H_m \dot{q}\right) \tag{5.25}$$

The results of the differentiation are called Non-Linear Convective Inertia matrices and contains the contribution to the dynamics of the Coriolis and Centrifugal forces. Thanks to SPART these matrices were already written in a neat and comprehensible form, ready to be used in the dynamic model. The process used by SPART is different from usual Euler-Newton approach, it is based on it, but uses Decoupled Natural Orthogonal Complement matrix to obtain the Convective Inertia matrices. The whole matrix C is now computed and then it could be split into the 4 submatrices: the $[6 \times 6]$ C_0, the $[6 \times N]$ C_{0m}, the $[N \times 6]$ C_{m0} and the $[N \times N]$ C_m

$$C = N^T\left(M\dot{\mathcal{N}} + \dot{M}\mathcal{N}\right) \tag{5.26}$$

where $M = diag\left([M_0, M_1, ...M_N]^T\right)$, collects all the Inertia matrices of each body:

$$M_i = \begin{bmatrix} I_i & 0_{3,3} \\ 0_{3,3} & \mathbb{I}_{3,3} \end{bmatrix} \tag{5.27}$$

$$\dot{M}_i = \begin{bmatrix} \omega_i \times I_i & 0_{3,3} \\ 0_{3,3} & 0_{3,3} \end{bmatrix} \tag{5.28}$$

and $\mathcal{N}$ is the $[6(N+1) \times (N+6)]$natural orthogonal complement or velocity transformation matrix, composed of two submatrices:

$$\mathcal{N} = \mathcal{N}_l \mathcal{N}_d \tag{5.29}$$

$$\mathcal{N}_l = \begin{bmatrix} \mathbb{I}_{6,6} & 0_{6,6} & \cdots & 0_{6,6} \\ B_{10} & \mathbb{I}_{6,6} & \cdots & 0_{6,6} \\ \vdots & \vdots & \ddots & \vdots \\ B_{N0} & B_{N1} & \cdots & \mathbb{I}_{6,6} \end{bmatrix} \tag{5.30}$$

$$\mathcal{N}_d = \begin{bmatrix} P_0 & 0_{6,1} & \cdots & 0_{6,1} \\ 0_{6,6} & p_1 & \cdots & 0_{6,1} \\ \vdots & \vdots & \ddots & \vdots \\ 0_{6,6} & 0_{6,1} & \cdots & p_N \end{bmatrix} \tag{5.31}$$

$$\tag{5.32}$$

in the equations above appear two terms, $B_{i,j}$ and p_i with $i, j = 0...N$, which represents respectively a $[6 \times 6]$ twist propagation matrix and a $[1 \times 6]$ twist propagation vector (except P_0 which is a $[6 \times 6]$ matrix):

$$B_{i,0} = \begin{bmatrix} \mathbb{I}_{3,3} & 0_{3,3} \\ (r_0 - r_i)^{\times} & \mathbb{I}_{3,3} \end{bmatrix} \qquad \forall\, i = 1...N \tag{5.33}$$

$$B_{i,j} = \begin{bmatrix} \mathbb{I}_{3,3} & 0_{3,3} \\ (r_j - r_i)^{\times} & \mathbb{I}_{3,3} \end{bmatrix} \qquad \forall\, j = 1...N,\ \ \forall\, i = 1....N \tag{5.34}$$

$$P_0 = \begin{bmatrix} {}^{\mathcal{I}}R_0 & 0_{3,3} \\ 0_{3,3} & \mathbb{I}_{3,3} \end{bmatrix} \tag{5.35}$$

$$p_i = \begin{bmatrix} \hat{k}_i \\ \hat{k}_i \wedge a_i \end{bmatrix} \tag{5.36}$$

$$\tag{5.37}$$

$\dot{\mathcal{N}}$ is the missing element to completely outline C, which is the time derivative of $\mathcal{N}$ and could be obtained substituting $r_j - r_i$ terms with the related $v_j - v_i$.

5.3 Newton-Euler Formulation

This formulation, as written above, was used only to characterize the manipulator part of the dynamic equation 5.13, namely H_m and C_m, through a recursive algorithm .
Starting from the last results of section 5.1 it is possible to compute the velocities wrt the inertial frame, through a forward recursion, acting on each body of the manipulator:

$$i = 1....N$$

$$v_i = v_0 + \omega_0^{\times} \left(r_i - r_0\right) + \sum_{k=1}^{i} \left\{ \left[\hat{k}_k^{\times} \left(r_i - p_k\right)\right] \dot{q}_k \right\} \tag{5.38}$$

$$\omega_i = \omega_0 + \sum_{k=1}^{i} \left(\hat{k}_k \dot{q}_k\right) \tag{5.39}$$

where ω_0 and $\dot{v}_0$ are the velocities of the base spacecraft, while $\omega_k = \hat{k}_k \dot{q}_k$ is the angular rate of the kth body, taken as isolated, expressed with respect to the inertial frame. Then the acceleration could be computed:

$$\dot{\omega}_i = \dot{\omega}_0 + \sum_{k=1}^{i} \left[\hat{k}_k \ddot{q}_k + \left(\omega_{k-1}^{\times} \hat{k}_k \dot{q}_k\right)\right] \tag{5.40}$$

$$\dot{v}_i = \dot{v}_0 + \dot{\omega}_0^{\times} \left(p_i - r_0\right) + \omega_0^{\times} \left[\omega_0^{\times} \left(p_i - r_0\right)\right] + \sum_{k=1}^{i-1} \left\{ \dot{\omega}_k^{\times} \left(p_i - p_k\right) + \omega_k^{\times} \left[\omega_k^{\times} \left(p_i - p_k\right)\right] \right\} \tag{5.41}$$

$$\dot{v}_{CMi} = \dot{v}_i + \dot{\omega}_i^{\times} a_i + \omega_i^{\times} \left(\omega_i^{\times} a_i\right) \tag{5.42}$$

where $\dot{\omega}_0$, which in the model received were set to 0 because the base was fixed; $\ddot{q}_i$ are the accelerations of each joint. As it could be seen from the equations above, the velocities and accelerations on each body result from the combination of those acting on the preceding, showing how each element of the manipulator is influenced by the previous.
Once obtained these parameters, it is possible to compute the forces and torques applied on each body, through a backward recursion, starting from the force applied

on the End-Effector:

$$i = 1...N$$

$$F_i = F_{EE} + \sum_{k=N}^{i} m_i \dot{v}_{CMi} - m_i g \tag{5.43}$$

$$N_i = N_{EE} + \sum_{k=N}^{i} F_k \wedge a_k + F_{k+1} \wedge b_k + I_k \dot{\omega}_k + \omega_k \wedge I_i \omega_i \tag{5.44}$$

$$M_i = N_i \hat{k}_i \tag{5.45}$$

$$\psi = [N_i, F_i] - [M_i \hat{k}_i, 0, 0, 0] \tag{5.46}$$

where F_i and N_i are the forces and torques applied by body i on body $i-1$, ψ is the restraining reaction on the joint; M_i are the torques acting on the ith joint, they are computed as the projection of the N_i on the z axis $(\hat{k}_i)$ of the local frame, because the joint is constrained about the other directions.
The uncoupled dynamic equation of the manipulator related to this formulation, in absence of friction is:

$$M = H_m \ddot{q} + C_m \dot{q} \tag{5.47}$$

where M is the vector containing all M_i.

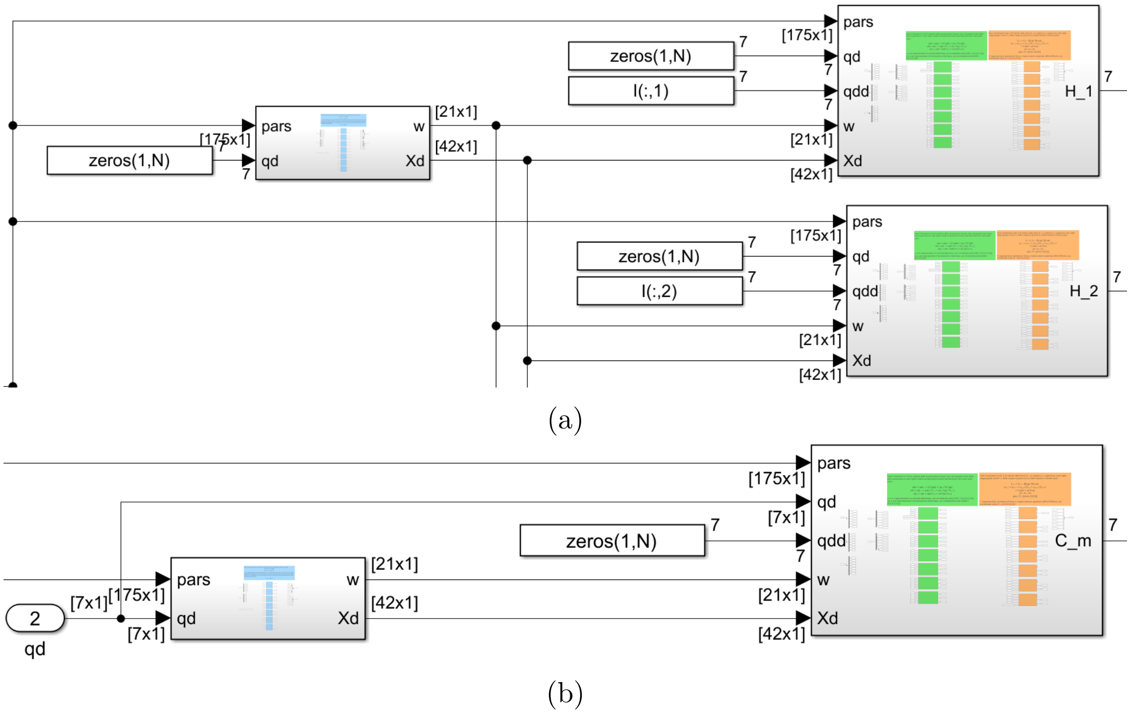

Figure 5.3: (a) shows the simulink blocks computing the first two column of H_m, while (b) computes the $C_m\dot{q}$; the subsystem on the left perform a forward recursion to evaluate the velocities, on right are computed all the torques and forces, thorugh a backward recursion

Using different sets of $\ddot{q}_i$ and $\dot{q}_i$ to evaluate forces and torques, as in fig 5.3 a and 5.3 b, then resolving 5.47 allows the assessment of H_m and C_m; H_m is computed recursively assuming a null vector for the velocities, and a unitary versor for the accelerations:

$$\dot{q} = 0 \; \ddot{q} = [1,0,0,...0] \rightarrow M = H_{:,1} \tag{5.48}$$

$$\dot{q} = 0 \; \ddot{q} = [0,1,0,...0] \rightarrow M = H_{:,2} \tag{5.49}$$

$$\vdots$$

$$\dot{q} = 0 \; \ddot{q} = [0,0,0,...1] \rightarrow M = H_{:,N} \tag{5.50}$$

each $H_{:,i}$ represent the ith column of the inertia matrix. Merging them together, the resulting H_m is produced; because both the formulation were used in the model, it was verified the matching between the manipulator inertia matrices evaluated in both ways, finding an error $\varepsilon \approx 10^{-14}$ which confirmed the equivalence between the two formulation. On the other hand, C_m is evaluated setting all the $\ddot{q}_i$ to zero and using the $\dot{q}$ obtained from the integration of 5.13:

$$\dot{q} = \dot{q} \; \ddot{q} = 0 \rightarrow M = C_m\dot{q} \tag{5.51}$$

in this case, instead of a matrix, is directly computed the $[1 \times N]$ $C_m\dot{q}$ vector; to include this element in 5.13, the matrix containing all the C was split in two part and then recombined as follow:

$$\Big[\mathrm{C}\Big]\begin{Bmatrix}\dot{x}\\ \dot{q}\end{Bmatrix} = \begin{bmatrix}C_0 & C_{0m}\\ C_{m0} & 0\end{bmatrix}\begin{Bmatrix}\dot{x}\\ \dot{q}\end{Bmatrix} + \begin{bmatrix}0\\ C_m\dot{q}\end{bmatrix} \tag{5.52}$$

where C_0, C_{0m}, and C_{m0} were computed through SPART.
Once higlighted all the physical properties of the system, is necessary to discuss the control modes used for commanding the manipulator.

5.4 Control Modes

The control system is responsible of generating the joint torque, used to perform the desired operation. As was introduced in chapter 4, this manipulator has three possible control modes:

- Joint Control (Direct Kynematics)
- Cartesian Control (Inverse Kynematics)

The first one, described in fig 5.4, exploits a simple PD (Proportional Derivative) control: the vector of joint positions q is compared to the desired position vector, $q_\star$; the output error, multiplied by a proportional gain K_P, is then used as input for a speed loop with derivative gain K_D, which output is considered as τ input of the dynamic model. This control technique is often used during deployment and retreat phases in which is not required neither a particular End-Effector position, either high precision tasks.

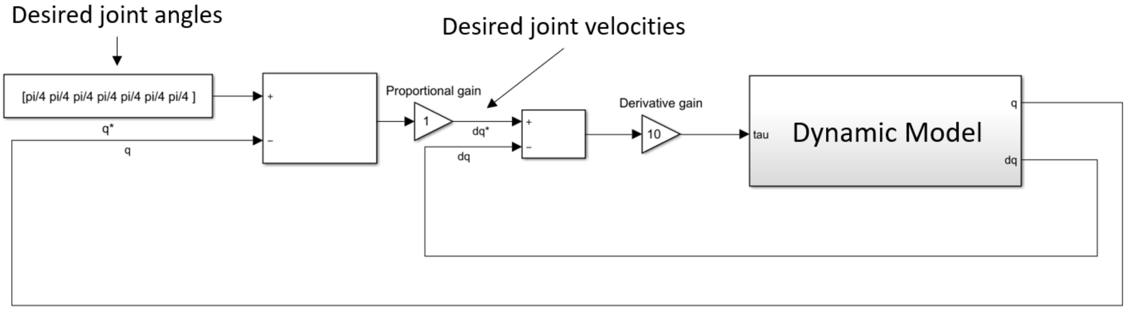

Figure 5.4: Direct Kynematics control diagram

The second one allows the user to move the End-Effector to a desired position with a desired orientation. This method exploits the GJM (Generalized Jacobian

Matrix) approach to find the required $\dot{q}$ to reach the desired End-Effector position. The joint velocities are computed as follows:

$$J\dot{q} = \begin{bmatrix} \omega_{EE} \\ v_{EE} \end{bmatrix} \tag{5.53}$$

$$\dot{q} = J^{-1} \begin{bmatrix} \omega_{EE} \\ v_{EE} \end{bmatrix} \tag{5.54}$$

where

$$J\dot{q} = J_0 \dot{x}_0 + J_m \dot{q} \tag{5.55}$$

$$J_0 = \begin{bmatrix} \mathbb{I}_{3,3} & -x_{0,EE}^{\times} \\ 0_{3,3} & \mathbb{I}_{3,3} \end{bmatrix} \tag{5.56}$$

$$J_m = \begin{bmatrix} \hat{k}_1 \left(p_{EE} - p_1\right) & \cdots & \hat{k}_N \left(p_{EE} - p_N\right) \\ \hat{k}_1 & \cdots & \hat{k}_N \end{bmatrix} \tag{5.57}$$

More specifically, it is present an outer proportional loop, in which the desired orientation and position of the end effector are compared to the current ones, the reulting error is then multiplied by a proportional gain and is used as velocity reference to get the set of desired joint velocities, through GJM approach as in equation 5.54. Once obtained the reference joint speeds is possible to find the necessary torque for moving each joint, so that the End-Effector reaches its assigned target, comparing the $\dot{q}$ to current ones and passing the error through a derivative gain.

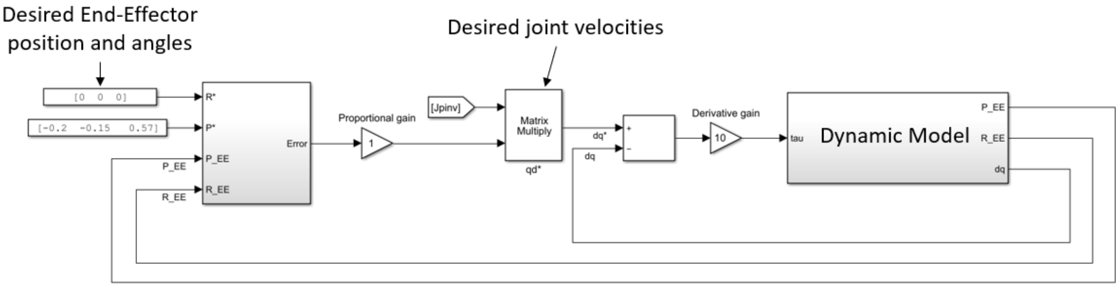

Figure 5.5: Inverse Kynematics control diagram, here J^{-1} is termed as *Jpinv*

Once defined all the elements composing the system, is possible to go ahead with the analisys of some simulations.

Chapter 6

Simulations Results

In order to study the dynamic interactions between the base-spacecraft and the manipulator, different simulations are performed. The analysis is focused on the reaction forces acting on the base, due to the manipulator movement, in order to provide a preliminary assessment with simplified control laws. For this purpose the disturbances induced on the base are evaluated as follows:

$$\tau = I_0 \dot{\omega_0} \tag{6.1}$$

where $\dot{\omega_0}$ are the base's angular accelerations caused by the motion of the joints and I_0 is its inertia.
Two groups of simulations are presented below, showing the deployment phase and a tracking phase, in which the End-Effector of the manipulator has to follow a moving target.

6.1 Simulations configurations

The 7 degrees of freedom of the arm could be grouped and divided into 3 articulations termed like human ones and having similar degrees of freedom. First 3 D.o.F.are grouped into a shoulder articulation which, as in tab. 6.3, has 3 possible rotations, then an elbow follows, with only a rotation possible, and finally there is a 3 D.o.F. wrist necessary to orient accurately the End-Effector.
The deployment phase starts from stowed position 6.1 (a) and ends into an extended one 6.1 (d), while the tracking phase starts from the end of the deployment and follows a moving target for 25 seconds to simulate the approach, identification and tracking of the grasping point. These simulations use different control techniques both for the arm and the base, depending on the task to carry out: direct kinematics for deployment and inverse kynematics for tracking regarding the arm, while the base is assumed perfectly controlled in the first case and floating in the second. The mass and geometric properties of the base and the arm are presented in the Table below:

	Base	Link 1	Link 2	Link 3
Lenght $[m]$		0,1189	0,1113	1,9276
Weight $[kg]$	1510	2,44	2,06	7,97

Table 6.1: Geometric and mass properties of the base and the links from 1 to 3

	Link 4	Link 5	Link 6	Link 7
Lenght $[m]$	1,8171	0,0690	0,0721	0,3709
Weight $[kg]$	7,73	0,90	0,90	3,57

Table 6.2: Geometric and mass properties of links 4 to 7

The first joint is placed on the surface of the base and it is 4.165 m far from base center of mass.

6.2 Deployment

The deployment is the first operation performed when approaching a target. Even if it could seem simple, it presents some criticalities because, once deployed, the arm should not hit the target nor interfere with the sensor for the acquisition of the target.
It is assumed that during the deployment the base is perfectly controlled (or rather, the disturbances computed as above are not applied to the spacecraft) and the arm starts from stowed position. Three phases, composed of several rotations of different joints, are necessary to completely deploy the arm. The whole sequence is presented in Table 6.3, with the detailed position of each joint. In addition to joint angles, Table 6.3 shows the time that the manipulator should take to perform each rotation, e.g. the shoulder roll and yaw rotation should be completed 50.6 seconds since the beginning of the simulation, or 25.1 seconds after the shoulder pitch rotation.

Rotation Sequence:	Joint Angles [°]	Time $[s]$
1) Stowed Configuration:	$[0, 0, 0, -180, 0, 0, 170]$	1
2) Shoulder Pitch Rotation:	$[0, 90, 0, -180, 0, 0, -180]$	25.5
3) Shoulder Roll and Yaw Rotation:	$[-90, 90, -90, -180, 0, 0, -180]$	50.6
4) Elbow Pitch, Shoulder Pitch and Wrist Yaw Rotation:	$[90, 140, -90, 90, 0, 0, 0]$	64.9

Table 6.3: Arm Deployment Sequence

Figure 6.1 depicts the deployment sequence, the represented spacecraft does not correspond to the real one, as well as for the arm, but it is useful to clearly outline the whole phase. In particular the mass and inertia properties used during the simulations refers to smaller and simpler chaser.

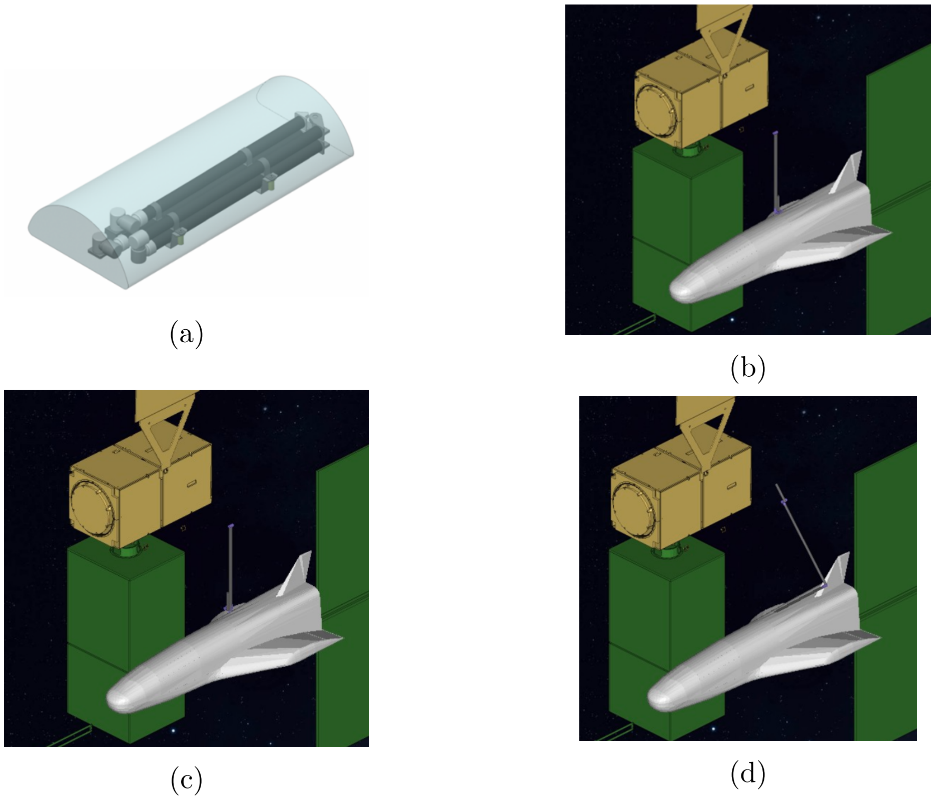

(a)

(b)

(c)

(d)

Figure 6.1: Here is shown the deployment sequence for the manipulator, starting from stowed configuration (a), is firstly performed a shoulder pitch rotation (b) follwed by roll and yaw rotation (c) and finally the elbow pitch rotation (d) - Courtesy of TAS.

The whole process starts with a shoulder pitch rotation from 0° to 90°(fig 6.1 (b)), to pull the arm away from the spacecraft, combined with a small wrist yaw rotation (10° rotation). Afterwards shoulder roll and yaw rotations are carried out, both from 0° to $-90°$ tto orientate the elbow for the final phase(fig. 6.1 (c)). Finally, the arm is totally deployed, through the elbow pitch rotation (from $-180°$ to 0°), followed by shoulder pitch and wrist yaw, respectively from 90° to 140° and from $-180°$ to 0°, to reach the right End-Effector orientation (fig. 6.1 (d)). Despite what the Table 6.3 could suggest, different rotations occurring during the same phase, i.e. shoulder roll and yaw rotations , does not always take place with the same speed, but have different angular rates, to avoid possible kinematics singularities that could thwart the whole process.

Once established the deployment sequence, it was necessary to find suitable gains of the controller, to obtain a reasonable compromise between precision and timing of the rotation and reaction torques on base. Among all the tests, three sets of K_D and K_P, gave satisfying results, which are reported below:

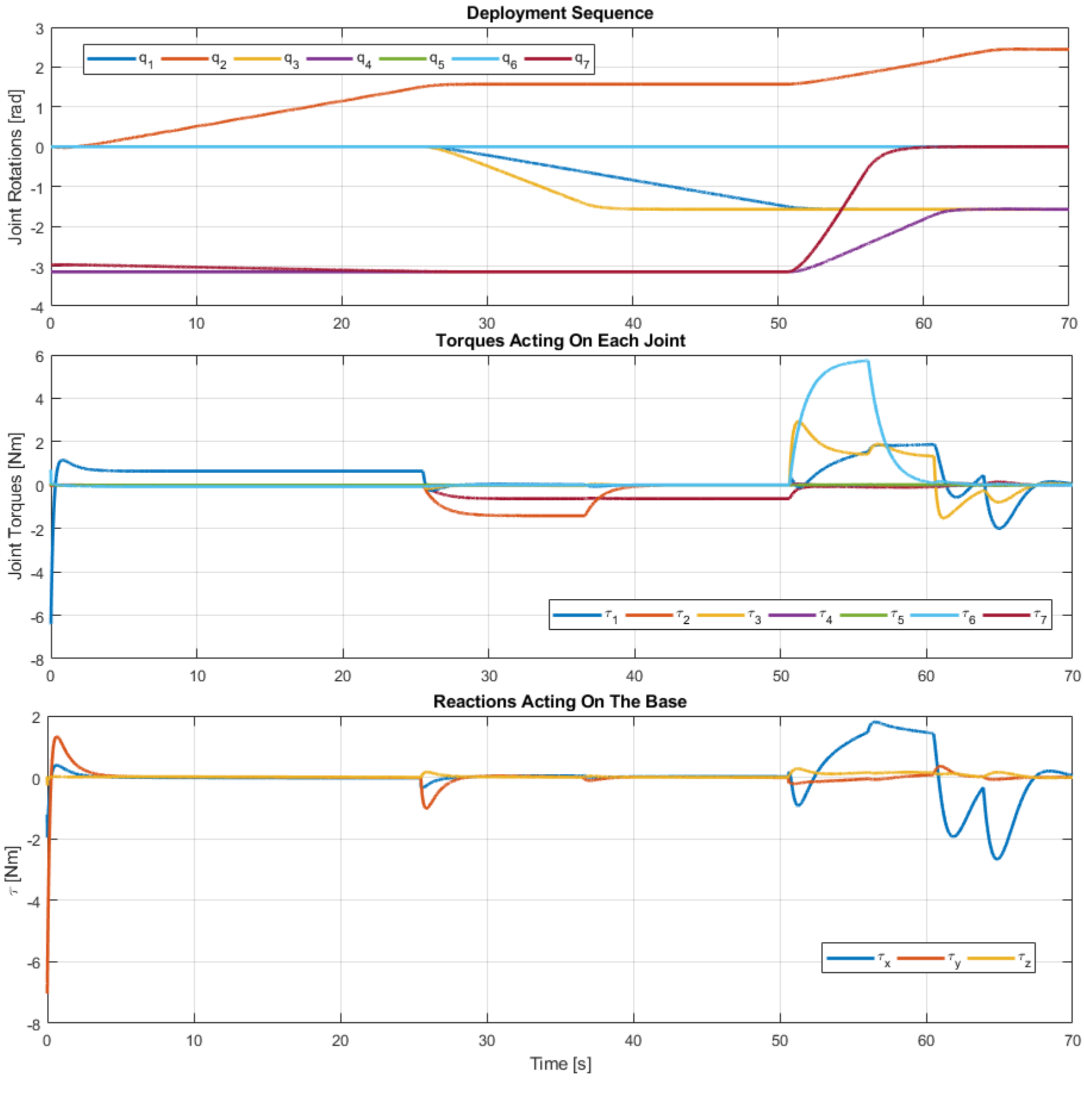

Figure 6.2: Deployment sequence with control gains $K_P = 1$ and $K_D = 100$

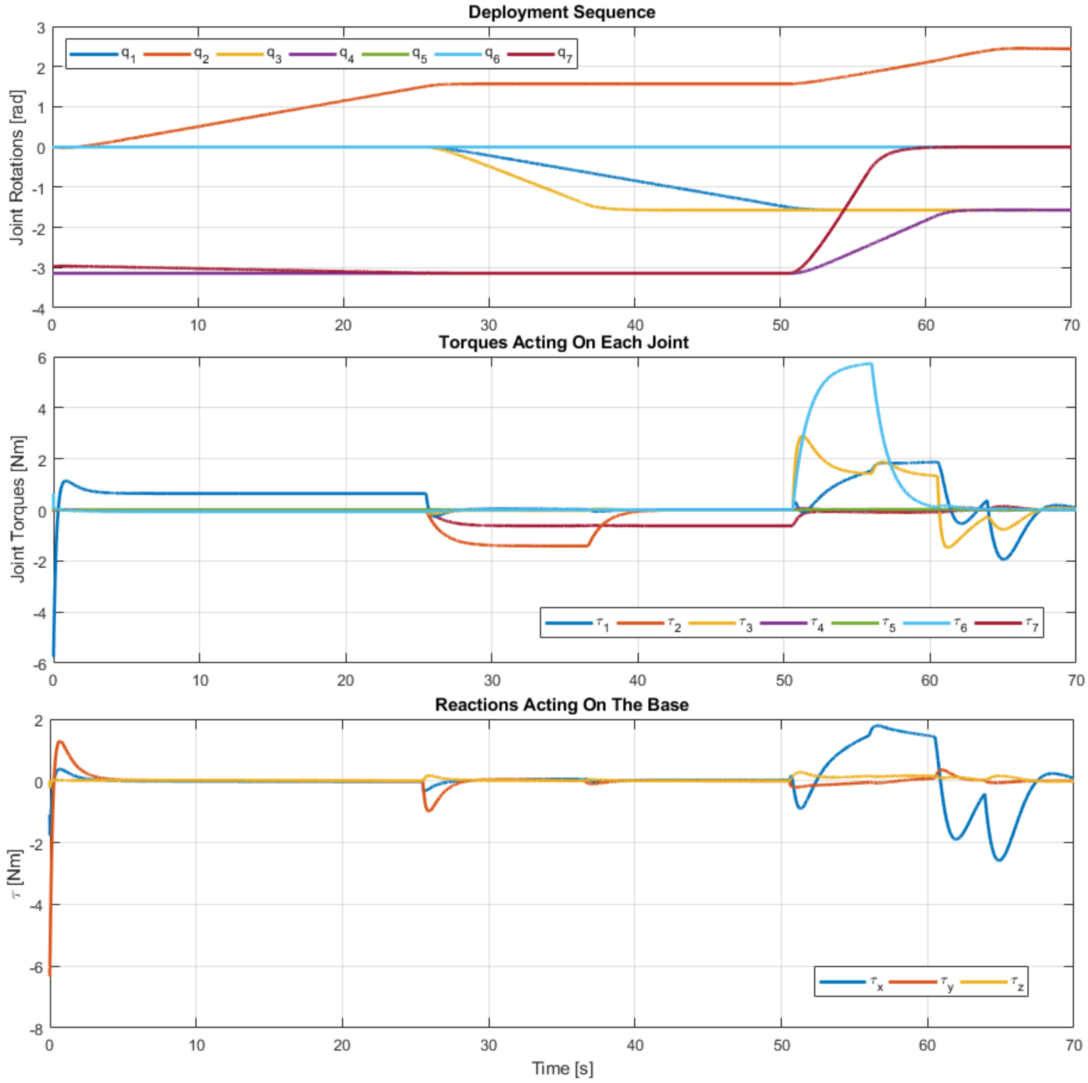

Figure 6.3: Deployment sequence with control gains $K_P = 0.7$ and $K_D = 90$

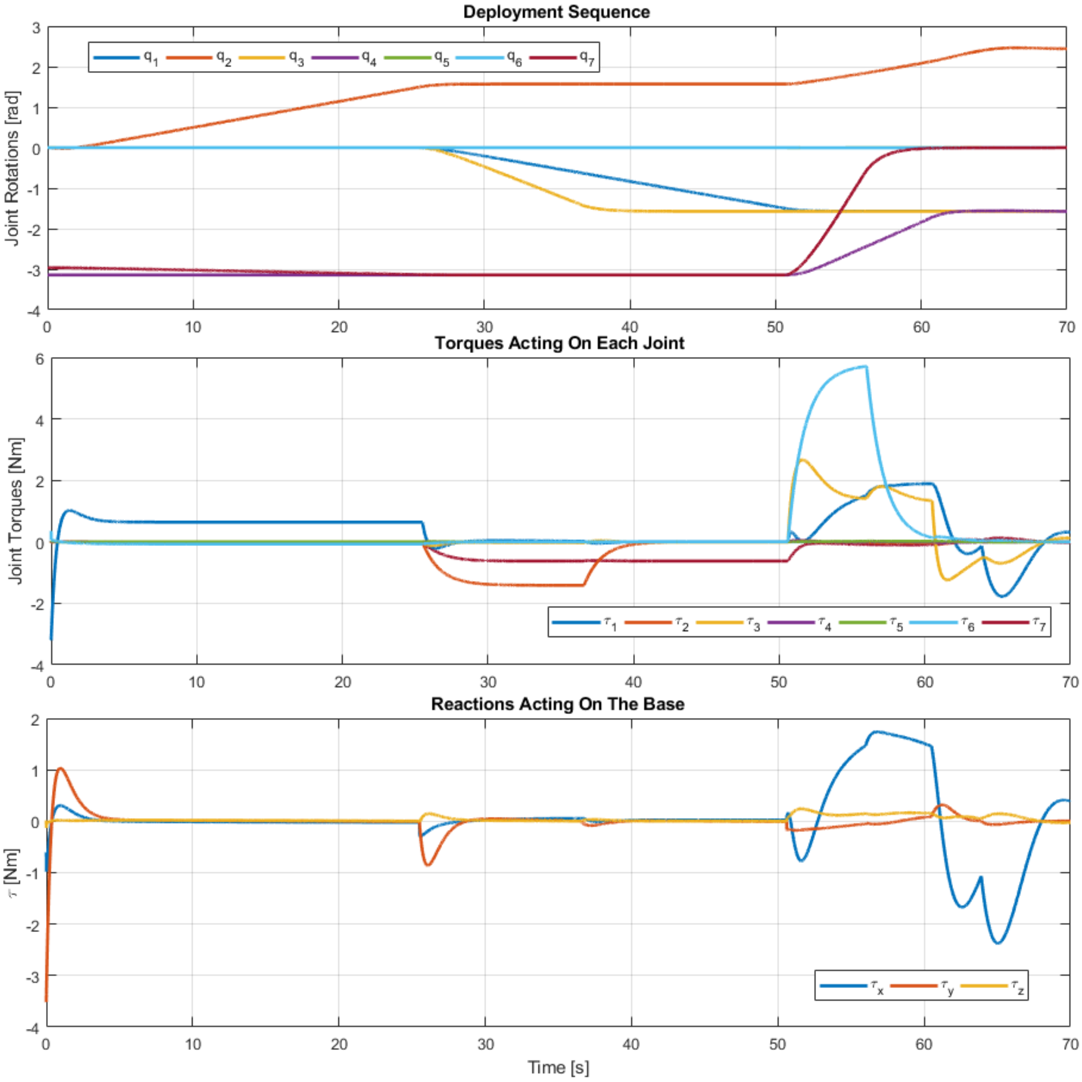

Figure 6.4: Deployment sequence with control gains $K_P = 0.5$ and $K_D = 50$

The images above highlight a torque peak, right after the beginning of the simulation. This is caused by the rotation of q_2 which moves the entire arm, similar to what happens after 50 s where the motion of q_1 and q_3 cause high τ_x on the base. To reduce these peaks, the gains are also reduced, especially K_D (results in Figure 6.4), but this led to slower lower rotation speed, which reflects in higher operational time. Therefore, Figures 6.2 and 6.3 present reasonable results where, on one hand the induced reactions are slightly higher, but on the other the operation requires less time to be performed. Anyway both fig. 6.2 and **??** shows torques which could be easily compensated by the control system of the base.

6.3 Tracking

The deployment, once completed, is followed by tracking phase, preparatory for the capture and necessary for identifying the correct pose of the grasping point and move the End effector close to it. To not interfere with the manipulator's motion, the base is not controlled anymore and it is free to float in space. A combined control between spacecraft and manipulator could be implemented to optimize the operation, but for the purpose of study it was out of scope.
The movement is controlled through inverse kinematics: given the position and orientation that the End-Effector has to reach with respect to to the inertial frame, via Eq. (5.54), the related joint angular rates and joint angles are computed. This maneuver is composed of two phases: a first approach to $\approx 50\ cm$ to evaluate the current pose of the grasping point and a second approach to $\approx 5\ cm$ close to the target, where the control mode switches from inverse kinematics to impedance control (not simulated here). The whole sequence is provided in the following Table:

Tracking Sequence	End-Effector Angles [°] and Positions [m]	Time [s]
Initial Approach	[−90, 0, 90, 4.43, 1.83, 3.15]	10
Grasping Point Acquisition	[−90, 0, 90, 4.43, 1.83, 3.15]	12
Final Approach	[−90, 0, 90, 4.43, 2.28, 3.15]	25

Table 6.4: Tracking Phase Sequence

Again as in the previous case, the time column is intended as the time elapsed since the beginning of the simulation. The target, on the other hand, is supposed to have a relative motion, both angular and linear, with respect to the chaser to create a more realistic environment. Image processing algorithms work efficiently when the relative angular motion stays within $-0.9 \leq \omega_{rel} \leq 0.9\ {}^{rad}\!/_{s}$ on all axis, hence it was selected $\omega_{rel} = [0.001,\ 0.02,\ 0.0015]\ {}^{rad}\!/_{s}$. The relative linear velocities, on the other side, are selected to simulate relative translational motion of two satellites very close to each other and in GEO orbits being constant and with the same module along the three directions equal to $0.01{}^{m}\!/_{s}$.
To study the performance of the manipulator during this operation, several simulations using different control gains were performed.

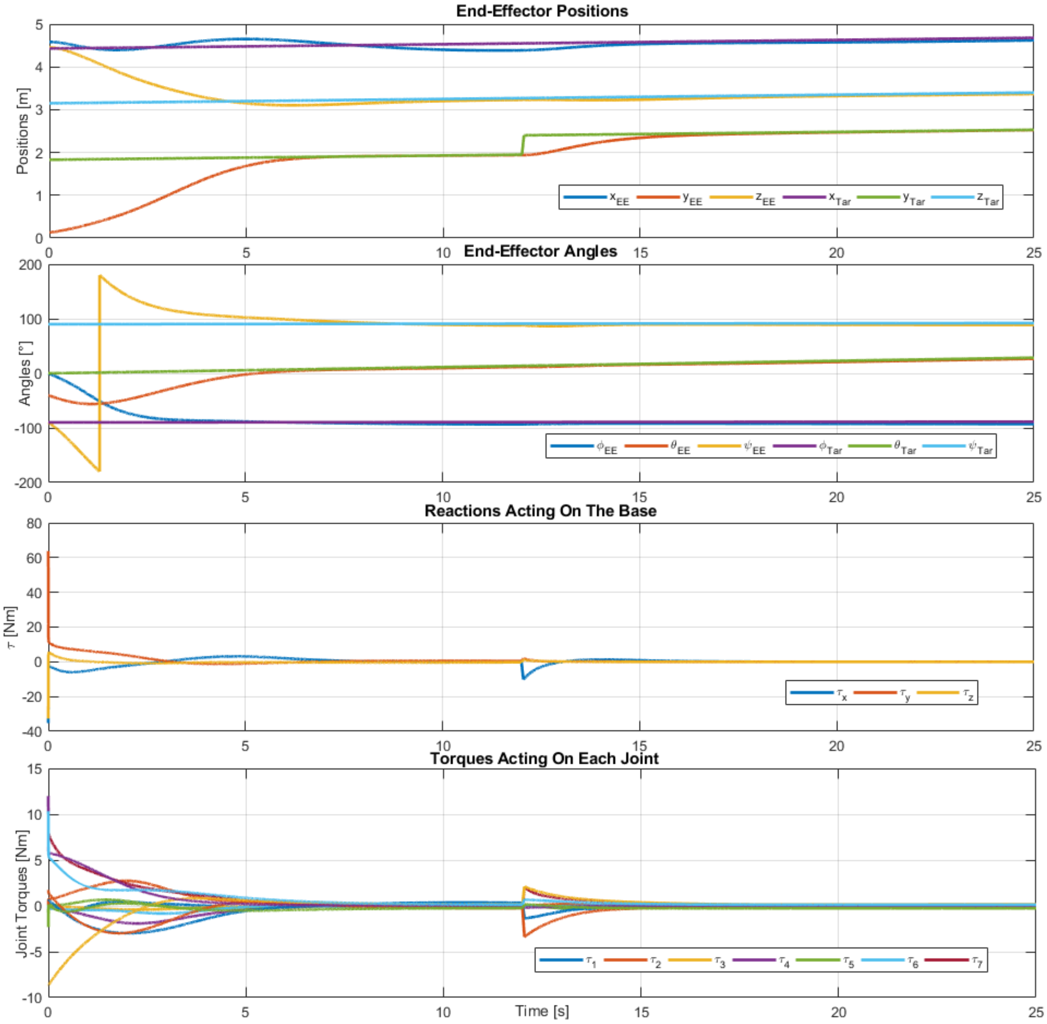

End-Effector Positions

End-Effector Angles

Reactions Acting On The Base

Torques Acting On Each Joint

Figure 6.5: Tracking phase with control gains $K_P = 1$ and $K_D = 10$

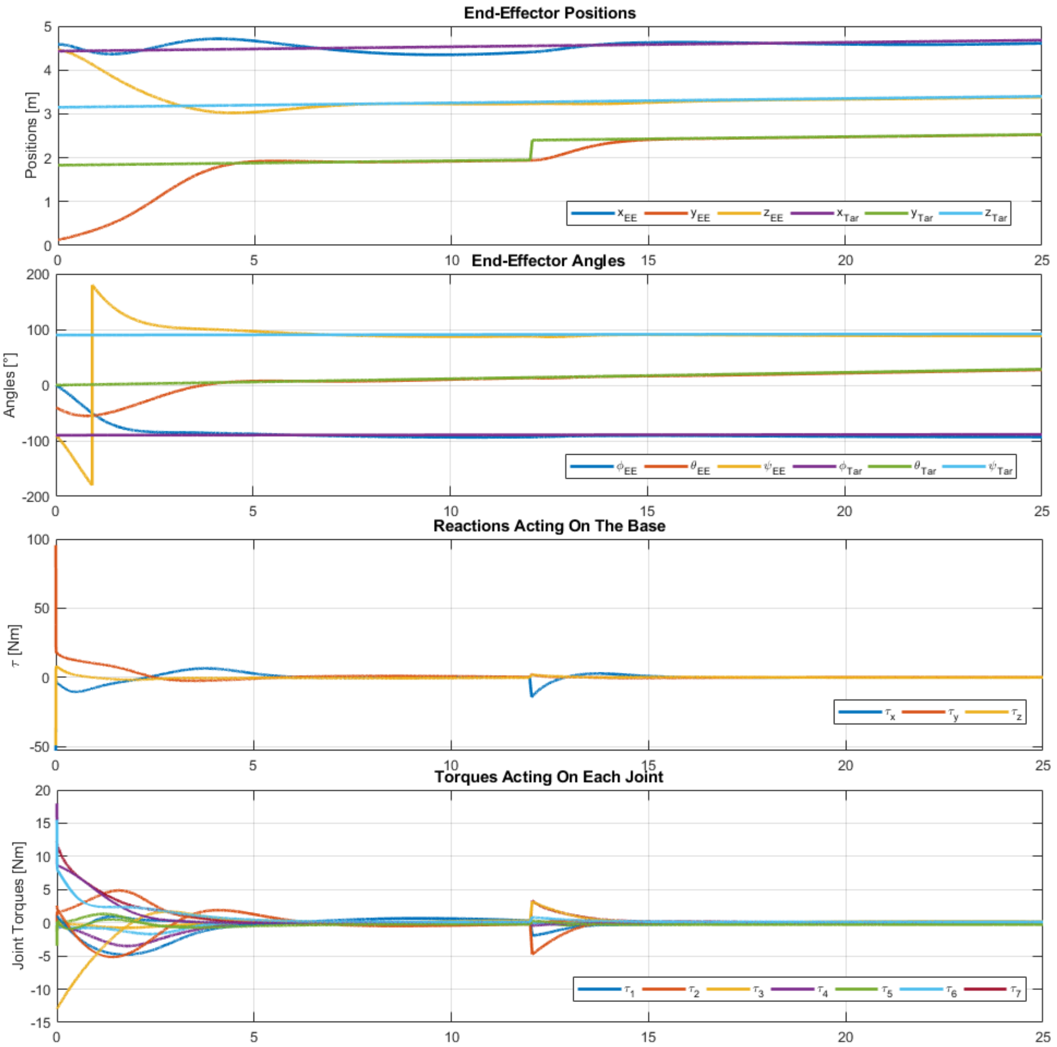

Figure 6.6: Tracking phase with control gains $K_P = 1.5$ and $K_D = 10$

The results show the End-effector successfully reaching the requested positions, but due to the relative motion between the two spacecraft, the manipulator has some difficulties in maintaining position along x-axis. It is possible to reduce this error, either increasing the derivative gain or decreasing the proportional one, but any of these choices brings its own drawbacks, as said in the previous section. The desired orientation, on the other hand, is easily reached by the End-Effector and the control system manages to follow the angular motion of the target without any remarkable concerns, regardless of the selected gains. In the end, the reactions acting on the base stay within acceptable limits, except for an initial peak, caused by simultaneous motion of all the joints, which lasts less than 0.01 seconds and therefore its effect could be mitigated without any particular difficulties.
As last result it is analyzed the base's angular displacement, to verify the impact

of the dynamic coupling. The angular displacement, as Figure 6.7 shows, is always less than 10 deg in any simulation. This means that, if the base mass and inertia properties are commensurate to the mounted manipulator, the spacecraft could perform fine operations without any specific issue.

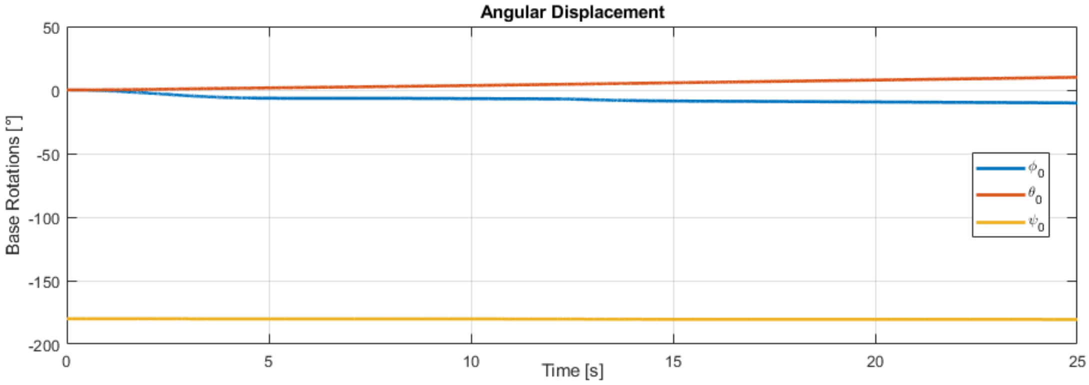

Figure 6.7: Rotations induced on the base during tracking phase

Chapter 7

Conclusions

Robotic missions represent next-generation services, aiming to reduce human impact on space environment. Among all the possible targets, to demonstrate the feasibility of rendez-vous and capture, were initially selected Galileo and Hipparcos, the former for reorbiting, the latter for deorbiting. The last one was selected, after a trade off, due to the lower cost in term of ΔV and due to the possibility to test life-extension/deorbiting kits, adding value to the scientific outcomes. The challenges arosen by the selected mission not only includes the rendez-vous and capture phases on uncooperative targets, but also the installation of external kits on unprepared surfaces. To perform these operation at least one robotic arm is required, which could be modelized using two conventional approaches Euler-Newton and Lagrange. Newton-Euler model is a recursive algorithm, which is better than Lagrange's in terms of computational efficiency, on the other hand Lagrangian approach is more comprehensible due to its systematic nature.

Both were used to model the space manipulator, Newton-Euler for the arm model, provided by an external company, Lagrange for base and for the system dynamics. Afterwards were studied the coupling effects between the manipulator and its base, performing different simulations. These showed that the coupling effect on the base, induced by the motion of the arm, could be easily managed by the control system's actuators. Particular attention, anyway, must be paid during manipulator path planning, in order to avoid collision with the target or the base and prevent kinematics singularities. In the future the model will have a more clear and complete integration between Lagrangian and Netwon-Euler formulations, and the C matrices will be computed, solving the derivatives in Eq.5.23, to optimize computational efficiency.

In order to create a more realistic environment, external disturbances, such as the gravity gradient, solar radiation pressure and, in case of LEO scenario, atmospheric drag, will be added. The control system, in the end, will be upgraded to have finer manipulator movements and a better control of the base in response to manipulator's disturbances.

Bibliography

[1] Yoshida, K., and Umetani, Y. (1993). “Control of space manipulators with generalized Jacobian,” in Space Robotics: Dynamics and Control, eds Y. Xu and T. Kanade (Boston, MA: Springer), 165–204.

[2] Stieber, M. E., Trudel, C. P., and Hunter, D. G. (1997). “Robotic systems for the international space station,” in Proceedings of the 1997 IEEE International Conference on Robotics and Automation (Albuquerque, NM: IEEE), 3068–3073.

[3] Sato, N., and Wakabayashi, Y. (2001). “JEMRMS design features and topics from testing,” in Proceeding of the 6th International Symposium on Artificial Intelligence and Robotics & Automation in Space: i-SAIRAS 2001 (St-Hubert, QC: CSA).

[4] Dreyer, L. (2009). “Latest Developments on SpaceX’s Falcon 1 and Falcon 9 Launch Vehicles and Dragon Spacecraft,” in IEEE Aerospace Conference (Big Sky, MT: IEEE).

[5] Ueda, S., Kasai, T., and Uematsu, H. (2010). “HTV rendezvous technique and GN&C design evaluation based on 1st Flight on-orbit operation result,” in AIAA/AAS Astrodynamics Specialist Conference, Guidance, Navigation, and Control and Co-located Conferences (Toronto, ON: AIAA), 1–12.

[6] Bain, M. E. (2010). “Cygnus: back to the future - applying commercial program lessons learned,” in AIAA SPACE 2010 Conference & Exposition (Anaheim, CA: AIAA), 1–8.

[7] Oda,M. (2000). “Experiences and lessons learned fromthe ETS-VII robot satellite,” in Proceedings of the 2000 IEEE International Conference on Robotics & Automation (San Francisco, CA: IEEE), 914–919.

[8] Kennedy, F. G. (2008). “Orbital express: accomplishments and lessons learned,” in Proceedings of the AAS Guidance and Control Conference (Breckenridge, CO: Univelt), 575–586.

[9] Dubowsky, S., and Papadopoulos, E. (1993). The kinematics, dynamics, and control of free-flying and free-floating space robotics systems. IEEE Trans. Robotics Autom. 9, 531–543.

[10] Papadopoulos, E. G. (1990). On the Dynamics and Control of Space Manipulators. Ph.D. Dissertation, Cambridge, MA: Massachusetts Institute of

Technology.

[11] Umetani, Y., and Yoshida, K. (1989). "Resolved motion rate control of space manipulators with generalized Jacobian Matrix". IEEE Trans. Robotics Autom. 5, 303–314.

[12] Vafa, Z., and Dubowsky, S. (1987). “On the dynamics of manipulators in space using the virtual manipulator approach,” in IEEE International Conference on Robotics and Automation (Raleigh, NC).

[13] Yoshida, K., and Umetani, Y. (1993). “Control of space manipulators with generalized Jacobian, in Space Robotics: Dynamics and Control”, eds Y. Xu and T. Kanade (Boston, MA: Springer), 165–204.

[14] J. Virgili-Llop et al., “SPART: an open-source modeling and control toolkit for mobile-base robotic multibody systems with kinematic tree topologies,” https://github.com/NPS-SRL/SPART.

[15] Siciliano, B., Sciavicco, L., Villani, L., and Oriolo, G. (2009). "Robotics: Modelling, Planning and Control" (Rome, IT: Springer)

[16] Curtis, H.D. (2005). "Orbital Mechanics For Engineering Students" (Amsterdam, NL: Elsevier).

[17] Wilde M, Kwok Choon S, Grompone A and Romano M (2018) Equations of Motion of Free-Floating Spacecraft-Manipulator Systems: An Engineer’s Tutorial. Front. Robot. AI 5:41.

[18] Liou, J. C. and Shoots, D. (2010). “Orbital Debris Quarterly News” Volume 14, issue 2, publication of NASA Orbital Debris Program Office.

[19] Scalise, G., and Pellegrino, P. “SAPERE/STRONG OR B4-1.1 – PRIDE Robotics System Configuration” TNO-SPR-STR-0001-TASI, issue 2.

[20] 2018, “Request For An Outline Concept For The Removal Of An ESA Owne, Satellite To Demonstrate Commercial In-Orbit Servcices”, Thales Alenia Space Answer to ESA RFI EA-SSP-K-RFI-0001.